CNRS
*Centre National de la Recherche Scientifique*

INFN
*Istituto Nazionale di Fisica Nucleare*


# Simulations of Advanced Virgo recycling cavities and thermal effects

VIR-0148A-10

Gabriele Vajente[1], Julien Marque[2]
[1] *INFN sezione di Pisa and Pisa University*
[2] *European Gravitational Observatory*

*Issue:* 1
*Date:* February 23, 2010

VIRGO * A joint CNRS-INFN Project
Via E. Amaldi, I-56021 S. Stefano a Macerata - Cascina (Pisa)
Secretariat: Telephone (39) 050 752 521 * FAX (39) 050 752 550 * Email W3@virgo.infn.it

# Contents



# 1 Introduction

Advanced Virgo recycling cavity can be designed to have a good separation between different high order resonant modes (non-degenerate recycling cavity NDRC) or to be degenerate (marginally stable recycling cavity MSRC). Moreover the Fabry-Perot arm cavities can be bi-concave or plane-concave always maintaining a large spot size on both input and end mirrors. These different designs have been considered and many results of a modal simulation are reported in this note. The technique used for the simulation has been already described in a previous note [1].

All configurations have been tested against the presence of thermal lensing in the input test masses. No error in the arm cavity mirror radii of curvature has been considered.

# 2 Simulation principles

The field is described at all points inside the interferometer as a vector of coefficients in the basis of the arm cavities. The interferometer configuration is defined in the perfect case: both cavities are equal and the input beam is perfectly matched to them. The cavity parameters define the Hermite-Gauss basis.

In the case of marginally stable recycling cavities the beam mode is propagated to the recycling mirror and the optimal curvature of PR is computed. In this simulation the mirrors are thin objects, without substrate. Therefore the lensing effect of the input mirror substrate is not considered.

Non-degenerate cavities are simulated in two different ways. Initially the geometry of the cavity is assumed to be simply the same as in the marginally stable case, propagating the arm cavity mode. The stability of the recycling cavity is then enforced setting an ad-hoc Gouy phase for the cavity propagation. This gives a wrong optimal value for the PR mirror but it results in a optical behavior equivalent to the real cavity. In a second moment the real cavity folding telescope has been simulated to include if wanted astigmatism. The cavity mode is propagated to the PR or SR mirror using ABCD matrix formalism [2]. In this way the correct Gouy phases for the propagation are recovered. The astigmatic mode is then expressed as a development in terms of the symmetric mode well matched to the recycling mirror. This mode is obtained assuming the same telescope but with zero incidence angle. In reflection of the recycling mirror the beam is propagated back to the input mirror, again using ABCD matrices formalism, and there it is expressed again in the basis of the arm cavities.

Thermal effects in the input mirrors are described adding a thin lens element in front of the Fabry-Perot cavities. Different combination of focal lengths have been selected. A rough rule has been used to convert from power absorbed in the mirror and resulting focal length:

$$f = \frac{2700 \text{ m/W}}{P_{ABS}} \tag{2.1}$$

Assuming a nominal 0.3 ppm total absorption in the input mirror and a maximum of 1 MW of intra-cavity power, the maximum absorption is 300 mW, corresponding to a lens of 9 km.

All mirror and lens operators are tuned in order to maintain always the carrier $TEM_{00}$ mode at the same resonance condition, whatever the lensing or mismatch. Therefore if the microscopical mirror position is not tuned during any simulation, the carrier fundamental mode is always nominally resonant. However due to thermal effects, this turns out not to alway be the optimal working point. Therefore a working point optimization algorithm has been developed and normally applied to the simulation. In the case of power recycling only simulation, this algorithm consists in two main steps: first the PRCL degree of freedom is tuned looking for the point that maximizes the sideband powers inside the PRC; afterwards the CARM degree of freedom is tuned to maximize the carrier power inside the arm cavities. When signal recycling is added further optimization steps are needed: DARM is tuned to maintain the standard $TEM_{00}$ carrier power at dark port; then SRC is tuned to maximize the sensitivity at a given frequency (300 Hz) which corresponds to the point of maximum shot-noise limited sensitivity in the design.

The experience shows that if no optimization of the working point is performed the performances of all configurations in terms for example of recycling gains are quickly worsened as thermal effects increase.

All the numerical computations are performed using MATLAB code. The matrix operators for lenses and mirrors are computed via numerical integration on a square grid, typically 1 m in diameter, subdivided in 300x300 of 600x600 points. In this way border effects are negligible and the mirrors are effectively of infinite size. It is however possible to specify a finite size of the mirrors to simulate clipping loss effects.

Higher order modes with $n + m \leq 8$ have been used.

The simulaton results gives the full interferometer matrix response for unity input fields. Therefore the results shown here are for 1 W of input power.

# 3 Configuration parameters

### Common parameters

| | | |
|---|---|---|
| Input mirror power transmission | 0.0069 | to get a finesse of 888 |
| End mirror power transmission | 75 ppm | accounts for all round trip losses |
| Input mirror losses | 0 ppm | |
| End mirror losses | 0 ppm | |
| Total round trip losses | 75 ppm | |
| Power recycling mirror transmission | 0.04 | |
| Power recycling mirror losses | 0 | |
| Signal recycling mirror transmission | 0.11 | |
| Signal recycling mirror losses | 35 ppm | |
| DARM offset for DC read-out | $10^{-11}$ m | to get about 80 mW of carrier $TEM_{00}$ power at dark port |
| Signal recycling detuning | 0.15 rad | to optimize sensitivity at 300 Hz |

### Arm cavity parameters

| | **Bi-concave** | **Plane-concave** |
|---|---|---|
| Input mirror ROC | 1416 m | $\infty$ |
| End mirror ROC | 1646 m | 31579 m |
| Arm cavity length | 3000 | |

### Recycling cavity parameters

| | **MSRC** | **NDRC** |
|---|---|---|
| Power recycling cavity length | 11.952 m | 35.857 m |
| Signal recycling cavity length | 11.0 m | 31.872 m |
| Modulation frequency | 6270659 Hz | |
| Schnupp asymmetry | 0.03 m | |
| PRC Gouy phase | $\sim$ 0 deg | 19.3 deg |
| SRC Gouy phase | $\sim$ 0 deg | 20 deg |

### Real astigmatic non-degenerate recycling cavities

| | | |
|---|---|---|
| Power recycling cavity length | | 37.344 m |
| First modulation frequency | | 6020832 Hz |
| Second modulation frequency | | 54187479 Hz |
| Distances between mirrors | $L_1$ | 10.413 m |
| | $L_2$ | 10.7 m |
| | $L_3$ | 16.057 m |
| Mirror ROC | $R_2$ | -2.0 m |
| | $R_3$ | 23.0304 m |
| Angle of incidence | | 1.34 deg. |
| Signal recycling cavity length | | 35.961 m |
| Distances between mirrors | $L_1$ | 9.03 m |
| | $L_2$ | 10.7 m |
| | $L_3$ | 16.057 m |
| Mirror ROC | $R_2$ | -2.0 m |
| | $R_3$ | 23.0304 m |
| Angle of incidence | | 1.34 deg. |

The first modulation frequency has been chosen to be perfectly anti-resonant in the Fabry-Perot arm and also perfectly resonant in the power recycling cavity. The second modulation frequency must be a multiple of the first one. The signal recycling cavity length has been chosen to make the second modulation frequency resonant for zero detuning.

# 4 Power recycling cavity

The first sets of simulation compare the performances of MSRC and NDRC in both the bi-concave and plane-concave configurations for what concerns the power recycling cavity. In these simulations the signal recycling mirror is removed and the Schnupp asymmetry set to zero. The two input mirror thermal lenses are always equal (*common mode thermal lensing*). Therefore the simulation deals for all purposes with a double cavity.

These simulation have two goals. The first is to understand if there is any difference between the bi-concave and plane-concave for the same recycling cavity scheme. The second is to compare the performances of MSRC versus NDRC.

In all the following simulations thermal lensing is changed from null absorption to a maximum of 300 mW corresponding to a thermal lens of 9 km.

## 4.1 Marginally Stable Recycling Cavity

### 4.1.1 Bi-concave arm cavities

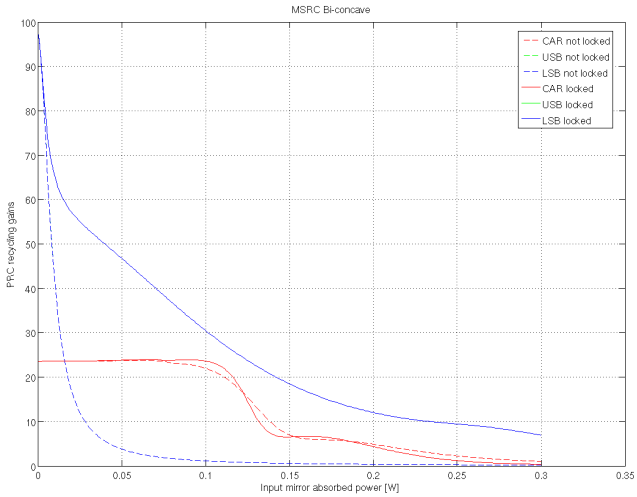


Figure 1: Recycling gains for carrier and sidebands, in the bi-concave MSRC case, with and without locking.

Fig. 1 shows the behavior of carrier and sidebands recycling gains (all modes) for the PRC as a function of the thermal effects. Dashed curves corresponds to the *not-locked* configuration: PRC and arm cavity lengths are not tuned when changing thermal effects, therefore always maintaining the $TEM_{00}$ nominally resonant. Solid curves shows the effect of the *locking* or in other words the tuning of the operating point, as explained in sec. 2.

It is interesting to separate the recycling gains in modes. Only the content in the fundamental $TEM_{00}$ mode turns out to be relevant. Indeed, RF sidebands are used for control purposes to generate error signal looking at their beating with the carrier. Since the carrier maintains an almost perfect $TEM_{00}$ mode, only the sidebands component in this mode really contributes to building the error signals. Fig. 2 shows again the total recycling

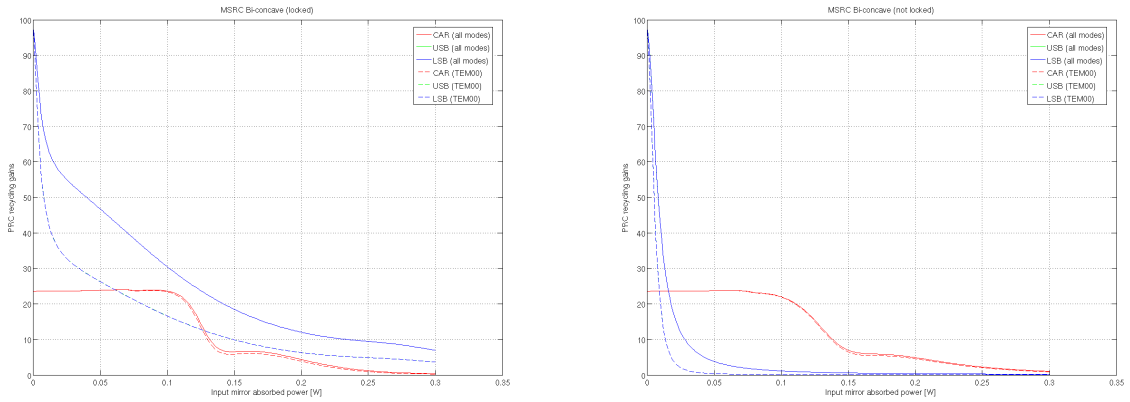


Figure 2: Recycling gains for carrier and sidebands, in the bi-concave MSRC case, subdivided in the $TEM_{00}$ and higher-order mode content. Left plot is for the locked configuration, right plot for the unlocked one.

gain but adding the projection in the $TEM_{00}$ mode. As anticipated, the carrier maintains an almost perfect mode shape, while the sideband gets a significant content in terms of high order modes.

The carrier maintains a high recycling gain (around 23) up to about 100 mW absorption, corresponding to about 27 km of focal length. The effect of the locking is negligible. Instead sideband drops quite faster. They start from a cold recycling gain of about 97 and if the ITF is not locked they reach 10 (in the $TEM_{00}$ mode) for 14 mW absorption, corresponding to about 200 km. However, if the working point is optimized the situation improves: sideband recycling gain in the fundamental mode is about 40 at 14 mW and 17 at 100 mW.

### 4.1.2 Plane-concave arm cavities

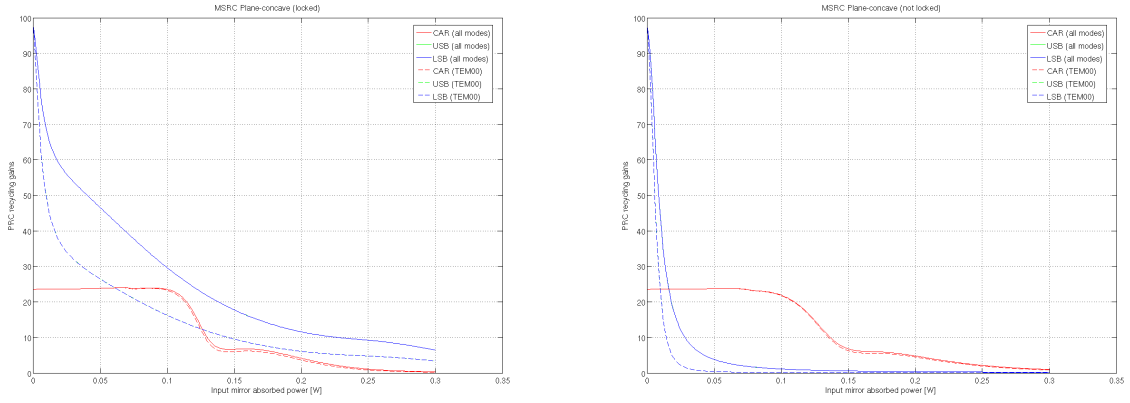


Figure 3: Recycling gains for carrier and sidebands, in the plane-concave MSRC case, subdivided in the $TEM_{00}$ and higher-order mode content. Left plot is for the locked configuration, right plot for the unlocked one.

The behavior in the plane-concave case is almost equal to the bi-concave one, as shown in fig. 3. The conclusion is that in the marginally-stable recycling gain the sensitivity to thermal effects is independent from the arm cavity geometry. If the thermal compensation system is able to reduce the residual lensing to a level corresponding to a focal of about 100 km (absorption of 27 mW), the $TEM_{00}$ recycling gain of the sidebands is reduced from the maximum possible value of about a factor 3, while the carrier is unaffected.

## 4.2 Non-Degenerate Recycling Cavity

### 4.2.1 Bi-concave arm cavities

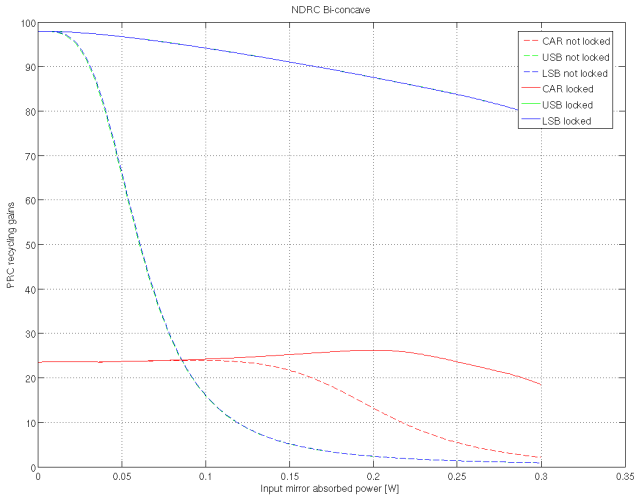


Figure 4: Recycling gains for carrier and sidebands, in the bi-concave NDRC case, with and without locking.

Fig. 4 shows the behavior of carrier and sidebands recycling gains (all modes) for the PRC as a function of the thermal effects. Dashed curves correspond to the *not-locked* configuration: PRC and arm cavity lengths are not tuned when changing thermal effects, therefore always maintaining the $TEM_{00}$ nominally resonant. Solid curves show the effect of the *locking* or in other words the tuning of the operating point, as explained in sec. 2.

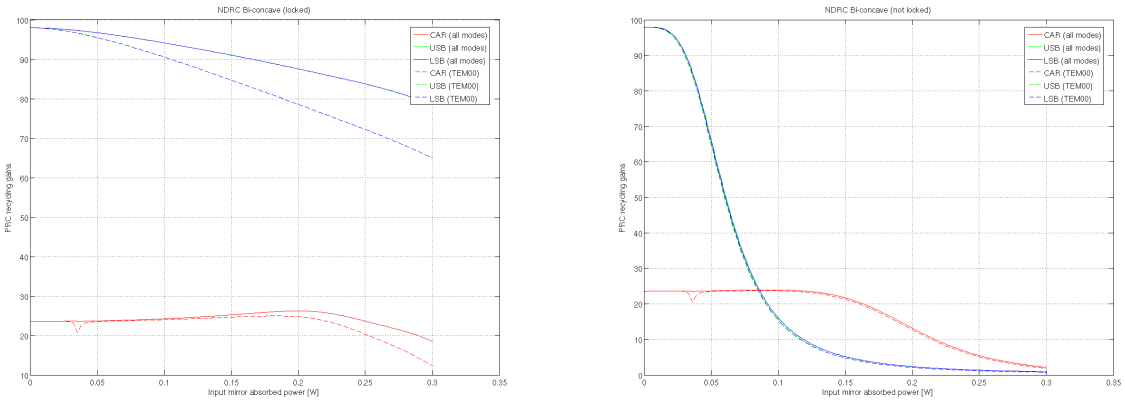


Figure 5: Recycling gains for carrier and sidebands, in the bi-concave NDRC case, subdivided in the $TEM_{00}$ and higher-order mode content. Left plot is for the locked configuration, right plot for the unlocked one.

Since the recycling cavity is non-degenerate and its resonant mode is assumed to be well matched to the arm one when there is no thermal lensing, the content of $TEM_{00}$ mode for all fields is always dominant, see fig. 7.

If the system is not locked, the carrier recycling gain remains high up to about 150 mW (corresponding to about 20 km. The sideband gain drops to low values faster than the carrier. Already at about 60 mW absorption (45 km) it reaches half of the maximum value and at 150 mW it drops to 5 percent.

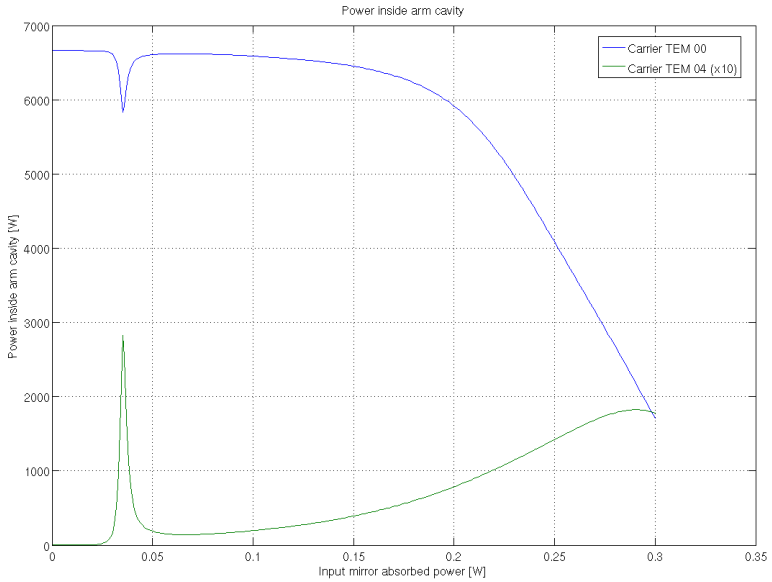


Figure 6: Power inside the in the bi-concave NDRC case, with and without locking.

The situation changes significantly if the system is locked. The carrier recycling gain remains high up to large lensing. Indeed it seems even to increase, but however as shown in fig. 6 the power inside the Fabry-Perot arm does not increase.

An interesting feature is the notch in arm and recycling carrier power around 35 mW absorption (corresponding to about 80 km of focal length). With this particular thermal lensing the modes of $4^{th}$ order get a dephasing in reflection of the aberrated arm cavity such to become resonant inside the power recycling cavity, thus extracting power from the fundamental mode. If only the propagation inside the recycling cavity is considered, the Gouy phase is such to move the $TEM_{04}$ mode close to anti-resonance if the $TEM_{00}$ mode is resonant. Inside the arm cavity the $TEM_{00}$ mode is resonant and the $TEM_{04}$ is not. There is therefore a phase difference close to 180 degrees between the reflection from the arm of the two modes. This moves the $TEM_{04}$ mode not far from resonance inside PRC. The addition of a thermal lens can introduce an additional dephasing of the $TEM_{04}$ mode in reflection of the arm and for the particular lensing one gets for 35 mW the mode can become resonant inside the PRC.

The locking procedure allows keeping a quite high recycling gain of sidebands up to quite large lensings. Indeed for 100 mW it drops only to 90 and for 200 mW to 78.

### 4.2.2 Plane-concave arm cavities

As in the marginally stable case, the behavior of NDRC is the almost the same for plane-concave and bi-concave arm configuration, see fig. 7. The only noticeable difference is the absence of any notch in the carrier recycling gain, since the fourth order modes never gets close to resonance.

## 4.3 Discussion

Fig. 8 shows a general comparison of the performances of all the configurations analyzed so far. The first evidence is that there is no significant difference between bi-concave and plane-concave configuration. Therefore the latter will be discarded in the following sections.

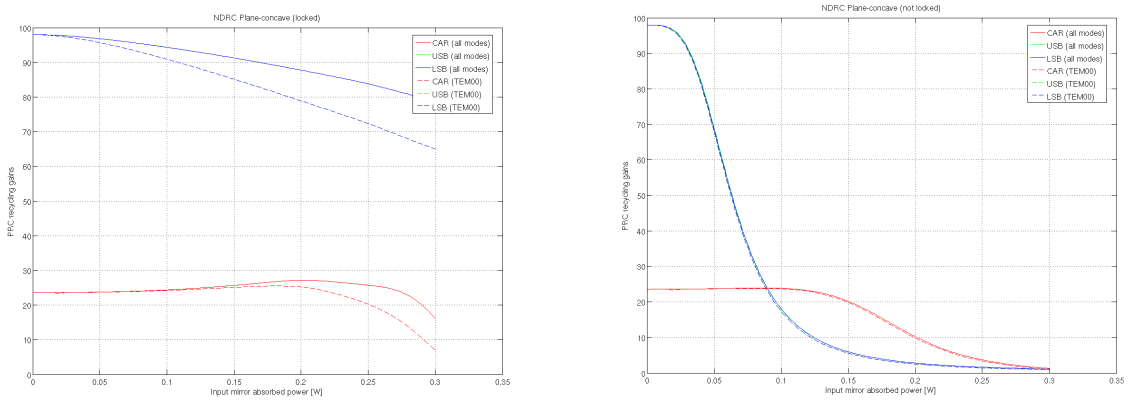


Figure 7: Recycling gains for carrier and sidebands, in the plane-concave NDRC case, subdivided in the $TEM_{00}$ and higher-order mode content. Left plot is for the locked configuration, right plot for the unlocked one.

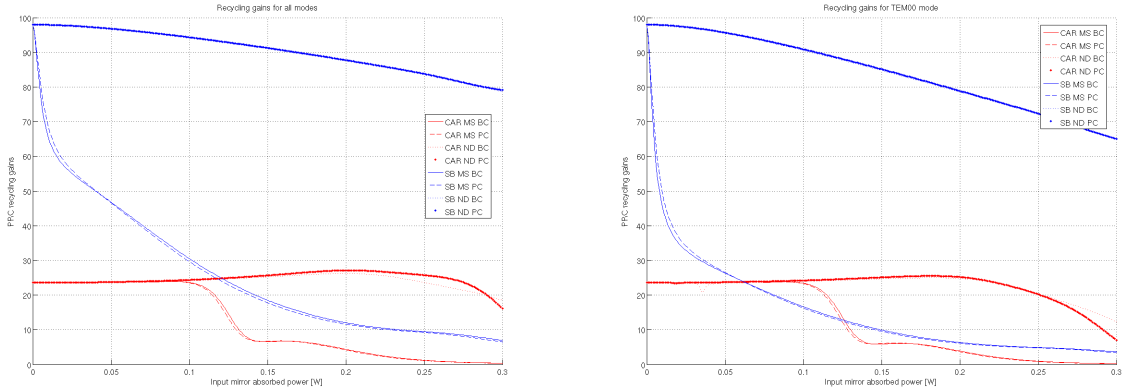


Figure 8: Comparison of recycling gains for all locked configurations. Blue curves refers to sidebands, red ones to carrier. Solid and dashed lines to MSRC, dotted to NDRC. Left plot gives the total power, right one only the $TEM_{00}$ component.

Differences between MSRC and NDRC are not very large concerning the carrier recycling gain. Instead the two cavities behave quite differently for what concerns the sidebands. Even with large thermal effects the NDRC maintains rather good sidebands recycling gains, while in the MSRC case the gain quickly drops down to about one third of the maximum before reaching 20 mW absorption (130 km) and then smoothly reduces to 10 at 150 mW (18 km) and to 6 at 200 mW (14 km). To reduce the loss of sideband recycling gain to 50 percent, thermal lensing should be kept below 10 mW or 270 km.

Fig. 9 shows the needed displacements of PRCL and CARM to maintain the double cavity locked at the optimal working point. It is clear that PRCL correction is smaller in the NDRC case.

# 5 Dual recycled interferometer - Common Mode Lensing

Using the optimized working point from the previous simulations (considering only the bi-concave configuration) it is possible to compute the effect of common mode lensing to the interferometer sensitivity, once the signal recycling mirror is added. The length of the signal recycling cavity is not important at this stage, provided it

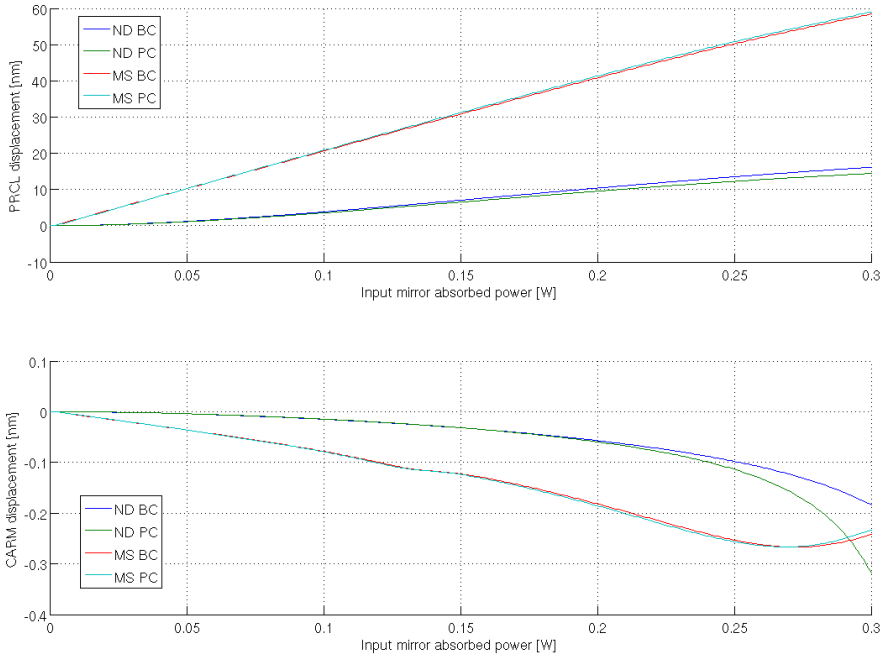


Figure 9: Comparison of the PRCL and CARM displacements needed to maintain the double cavity at the optimal working point.

remains smaller than some hundreds meters to avoid introducing significant dephasing for the signal sidebands.

The nominal signal recycling detuning is 0.15 rad [3] which corresponds to having the best shot-noise-limited sensitivity around 300 Hz.

The transfer function from DARM motion to the dark port carrier $TEM_{00}$ can be computed from the simulation as well as the static carrier $TEM_{00}$ power. The shot noise level is computed from this last value and calibrated in units of $h$.

Note that in these simulations radiation pressure effects are not considered. Therefore the computed DARM transfer function and the shot-noise-limited sensitivity are not correct at low frequency. In particular the quantum-noise-limited sensitivity of Advanced Virgo at full input power is supposed to be limited by radiation pressure below few tens of Hz [3].

## 5.1 Marginally Stable Recycling Cavity

The shot-noise-limited sensitivity changes significantly with common thermal effects if the position of the signal recycling mirror is not changed, see fig. 10. Looking at the sensitivity evolution it appears that the largest effect comes from a detuning of the signal recycling. Thermal effects changes the phase accumulated by signal sidebands and therefore maintaining the nominal SRC tuning does not allow to place the peak sensitivity always at the same frequency.

An optimization algorithm has been applied which tries to maximize the sensitivity at the frequency of the SRC dip by moving the SRC tuning. The result is shown in fig. 11. The low and high frequency sensitivity can be recovered for all lensings (up to 100 mW) as well as the position of the dip around 300 Hz. The only significant residual effect if the depth of the dip, which starts to be reduced when thermal lensing increases. For absorbed

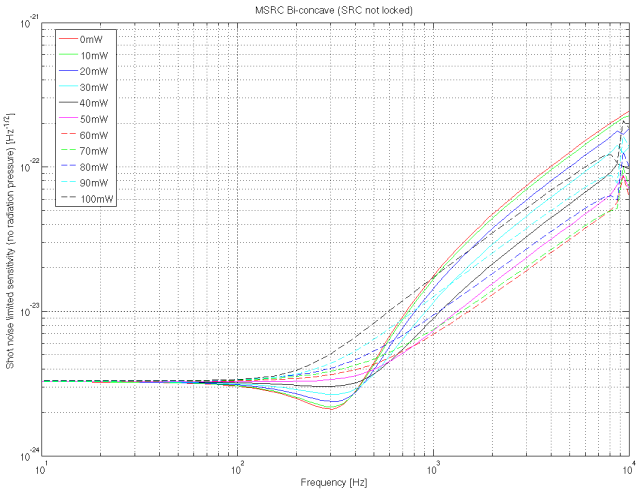


Figure 10: Evolution of the shot-noise limited sensitivity in the MSRC case, without re-tuning the signal recycling position.

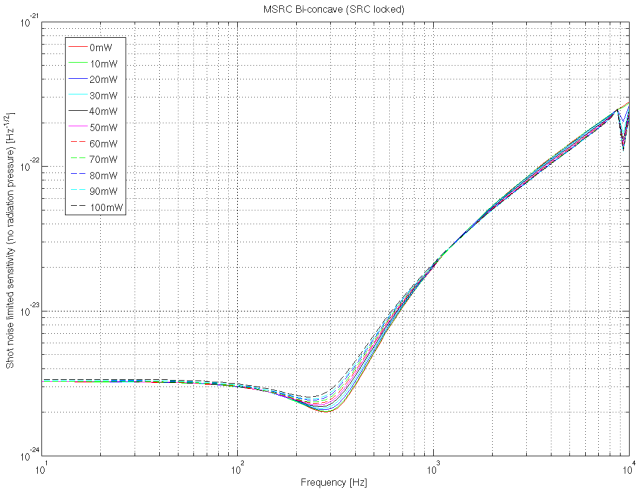


Figure 11: Evolution of the shot-noise limited sensitivity in the MSRC case, optimizing SRC tuning at each lensing value.

power lower than 20-30 mW (residual focal greater than 80 km) the loss in shot-noise-limited sensitivity at 300 Hz is smaller than 8 percent. For a lensing of 70 mW (40 km) the loss at 300 Hz is around 30 percent.

Fig. 12 shows how the optimal SRC tuning changes with thermal lensing. However, since the peak sensitivity is always placed roughly at the same frequency, it means that the real tuning which is defined by the signal sideband dephasing, is maintained constant with the optimization procedure. The reduction of gain at the signal recycling peak can be understood considering thermal effect as a source of losses through high order modes.

The effect of thermal lensing on the signal sidebands is definitely lower than on the radio-frequency sidebands, since the former are at least partially resonant inside the arm cavities.

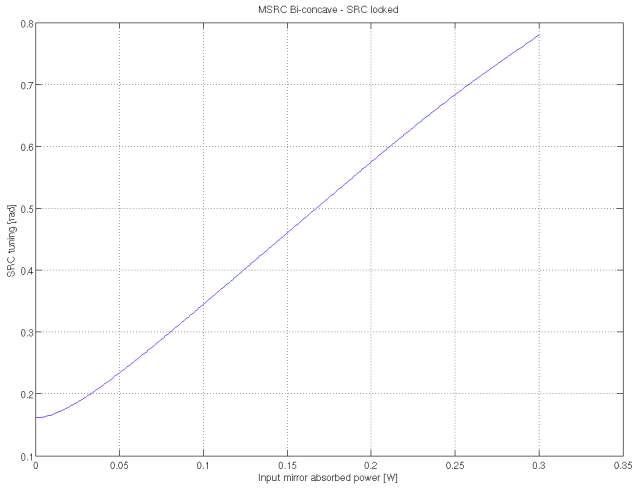


Figure 12: Optimal value for SRC tuning when different common mode thermal lensing are present (MSRC).

## 5.2 Non-Degenerate Recycling Cavity

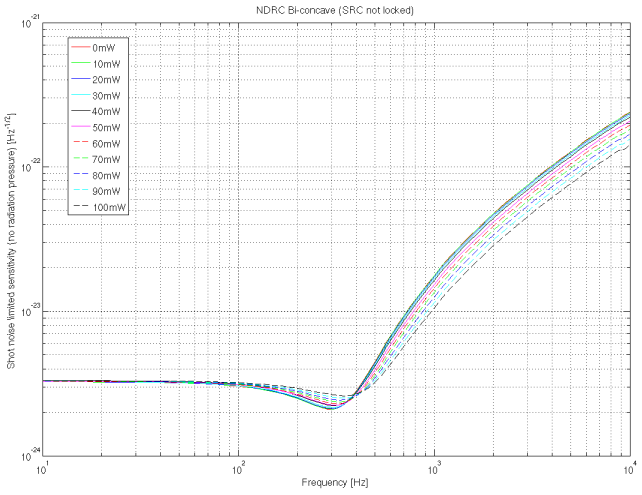


Figure 13: Evolution of the shot-noise limited sensitivity in the NDRC case, without re-tuning the signal recycling position.

Exactly as done for the MSRC, the optimized working positions computed in the double cavity simulations have been used as starting points for the computation of the interferometer shot-noise-limited sensitivity. Without optimizing the signal recycling tuning the result is shown in fig. 13. Again there is a mis-tuning effect, even if smaller than in the MSRC case. It is important to stress that so far no astigmatism has been introduced in the NDRC cavities.

When the SRC tuning is changed at each step to maximize the sensitivity around the 300 Hz peak, the cold interferometer sensitivity is almost fully recovered for every thermal lensing, see fig. 13. The re-tuning needed to recover a good sensitivity is smaller than in the MSRC case.

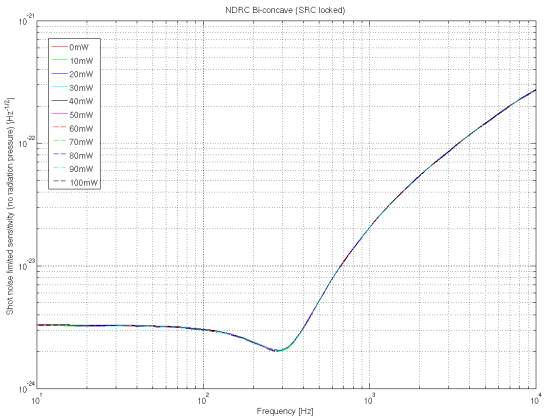


Figure 14: Evolution of the shot-noise limited sensitivity in the NDRC case, optimizing the SRC tuning.

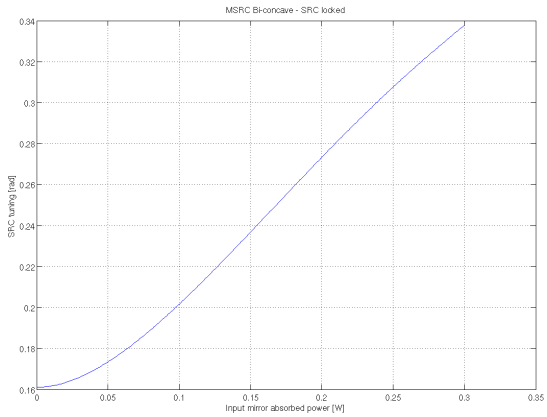


Figure 15: Optimal value for SRC tuning when different common mode thermal lensing are present (NDRC).

### 5.3 Discussion

Simulations show that in presence of common mode thermal effects, marginally stable recycling cavities show a not to large loss in sensitivity, provided the interferometer working point is properly optimized. This loss is mainly concentrated around the signal recycling sensitivity peak around 300 Hz. At that frequency residual thermal lens focal greater than 80 km ensures a shot-noise-limited sensitivity loss smaller than 8 percent. With a residual lens of 40 km the loss in shot-noise-limited sensitivity is about 30 percent.

Non-degenerate recycling cavities, *in presence of only common mode thermal effects and without astigmatism* allow a perfect recovering of the nominal shot-noise-limited sensitivity even for reasonably large thermal effects. However above about 150 mW of absorbed power carrier power inside arm cavities starts to drop and sensitivity is lost.

## 6 Dual recycled interferometer - Arbitrary Lensing

To study the effect of both common and differential mode lensing, the same simulations of the previous section have been repeated covering all possible values of the two input mirror absorptions from 0 to about 130 mW,

corresponding to focal lenses greater than about 20 km. The results are presented as maps of the two-dimensional lensing space: the x variable gives the level of the absorption in the north input mirror, the y variable the level of absorptions in the west input mirror. The upper and the right axis show corresponding residual focal lengths. In all the following maps the color scale as well as the contour plots shows the evolution of the analyzed variable as a function of the thermal lensing. Unless otherwise explicitly stated, the interferometer operating point is optimized for each bin of the map:

1. PRCL is tuned to maximize the sum of the power in the $TEM_{00}$ of the two sidebands, measured inside PRC;
2. CARM is then tuned in order to maximize the mean carrier $TEM_{00}$ power inside the two arms;
3. DARM is tuned in order to keep the dark fringe carrier $TEM_{00}$ power to the target value;
4. SRCL is then tuned looking for the maximum sensitivity in the region around 300 Hz.

## 6.1 Marginally Stable Recycling cavity

Carrier and sidebands recycling gains are shown in fig. 16. The dependence on common mode thermal lensing is clearly visible, while it seems there is no dependence on differential thermal lensing.

Fig. 17 shows the evolution of the power stored inside the arms and the total power at dark port (note that the input power is 1 W). The former shows again no dependence on differential lensing. The dark fringe power in the $TEM_{00}$ mode is kept constant by the DARM tuning, but the content in high order modes can change accordingly to differential thermal effects. This is intuitive since any differential thermal lensing will generate high order modes with opposite amplitudes in the two short Michelson arms. These differential fields are then perfectly transmitted to the dark port because of the dark fringe MICH locking condition.

Fig. 18 shows the corrections applied to the common mode degrees of freedom PRCL and CARM to optimize the interferometer working point. Again no dependence on differential mode lensing is present.

Fig. 19 shows DARM and SRCL corrections. Again the signal recycling tuning is changed to maintain the best possible sensitivity. Almost no dependence on the differential lensing is visible. DARM correction is instead depending mainly on the differential lensing, with a contribution also from the common lensing. The amount of this correction is in any case small.

The evolution of the sensitivity is shown in fig. 20 and 21, where the shot-noise-limited sensitivity of the interferometer is shown at different frequencies: 10, 100, 1000 and 300 Hz. The 10 Hz sensitivity is not considering the effect of radiation pressure, therefore it is not very meaningful. The plots are normalized to the sensitivity at that frequency without thermal effects: the value shown in the plots gives the percentual increase of shot-noise-limited sensitivity with respect to the cold state:

$$z = 100 \times \frac{h_{thermal}(f) - h_{cold}(f)}{h_{cold}(f)}$$

The loss in sensitivity is mainly depending on the common mode lensing. As already shown by the common mode only analysis of the previous sec. 5.1, the sensitivity worsening is moderate at all frequencies except around 300 Hz. With an average absorption smaller than 100 mW (27 km) the loss of sensitivity is smaller than 10% at 10, 100 and 1000 Hz.

The effect is larger around 300 Hz and it depends mainly on the quadratic sum of the two absorptions. With a residual lensing of the order 40 km the worsening is of the order of 27%. With 60 km the loss reduces to 17% and with 100 km to less than 10%. It is important to remember that these numbers give the increase of shot-noise only, not of the entire detector sensitivity: if around 300 Hz there are other sources of noise competitive in amplitude with shot noise (coating Brownian noise in Advanced Virgo is only 50% lower than shot noise at 300 Hz [3]) the effect on the total sensitivity is reduced.

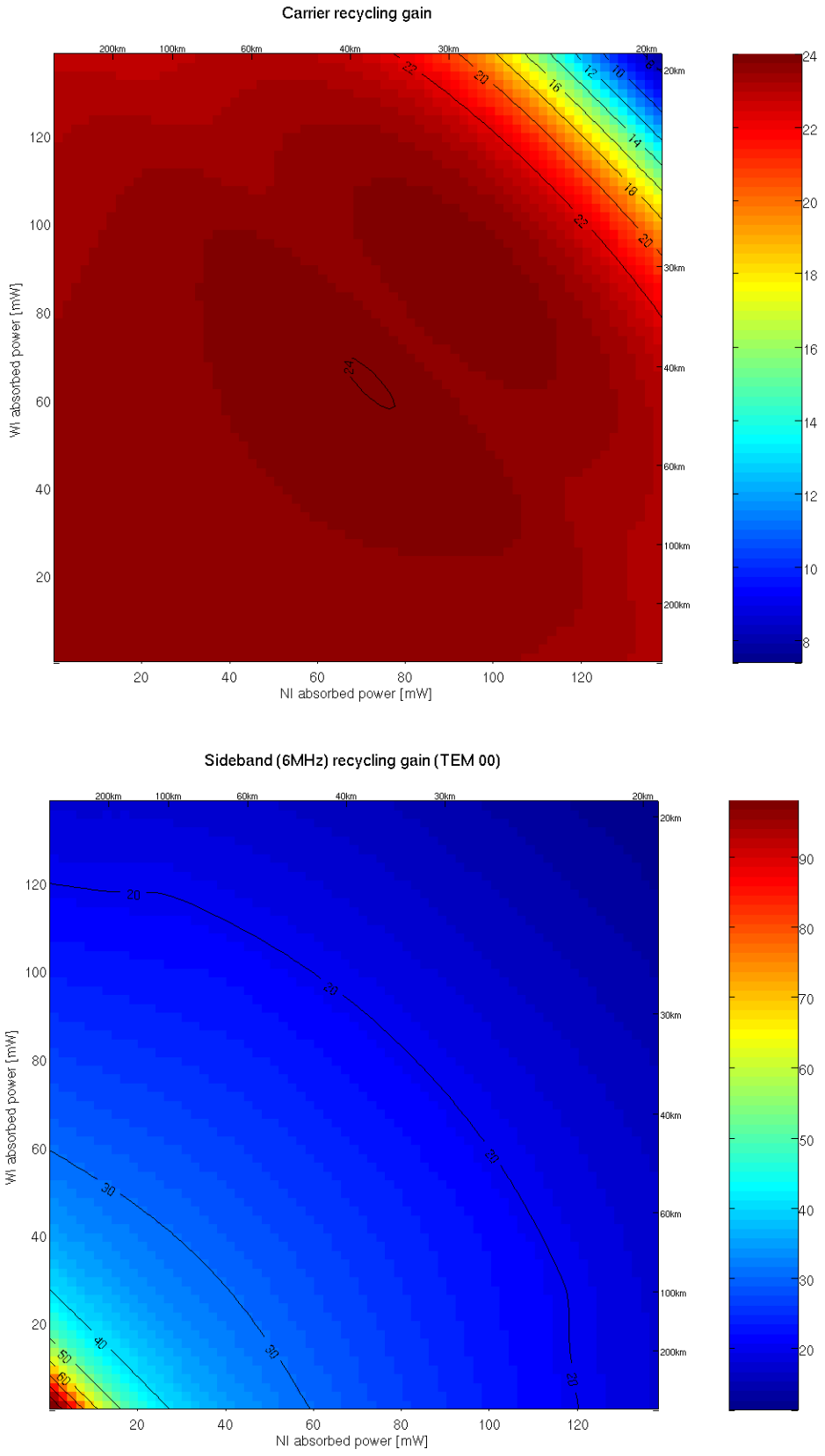


Figure 16: **MSRC.** Carrier (top) and sideband (bottom) recycling gain ($TEM_{00}$)

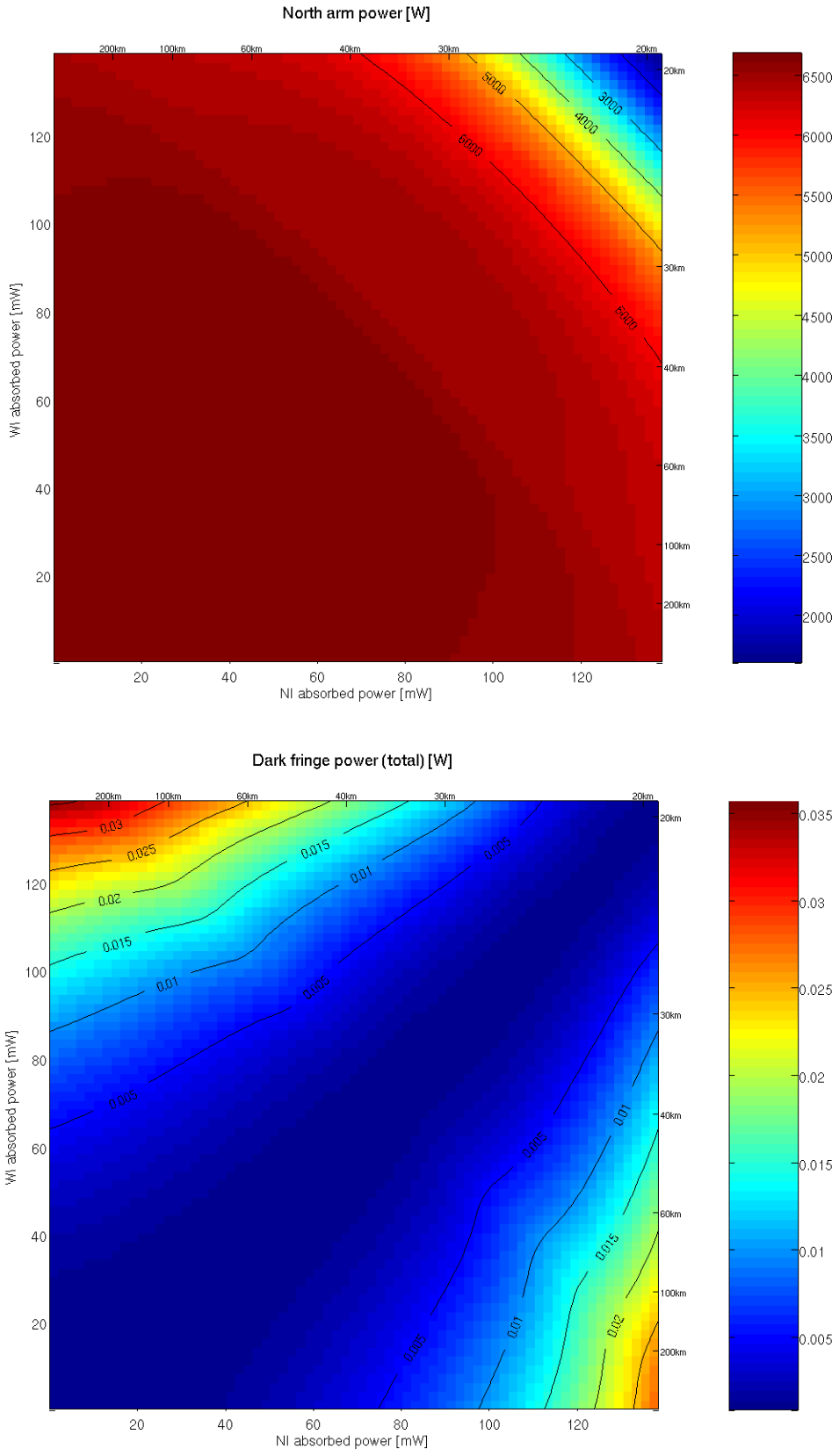


Figure 17: **MSRC.** Power inside north arm (top) and at dark port.

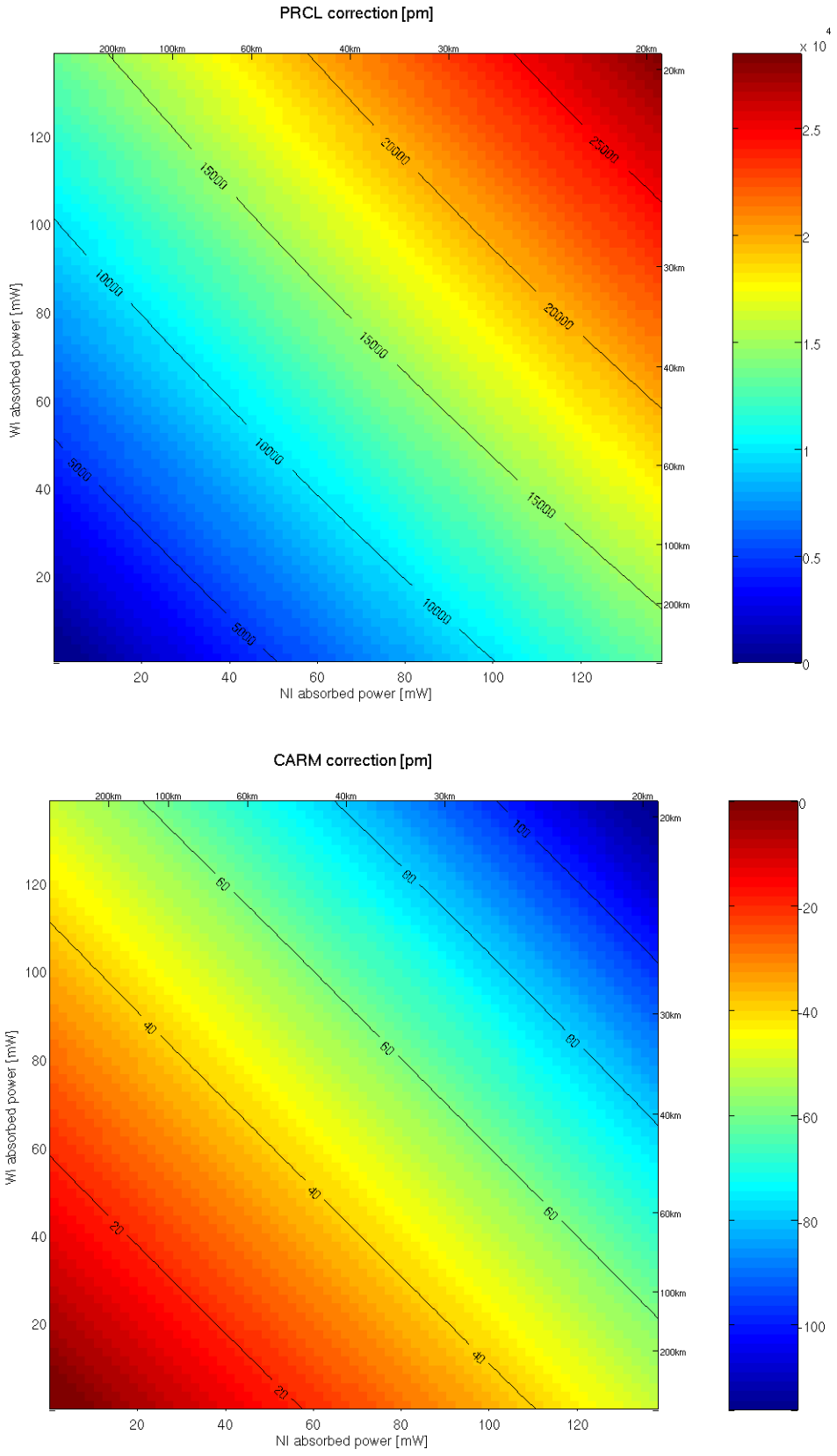


Figure 18: **MSRC.** PRCL (top) and CARM (bottom) corrections.

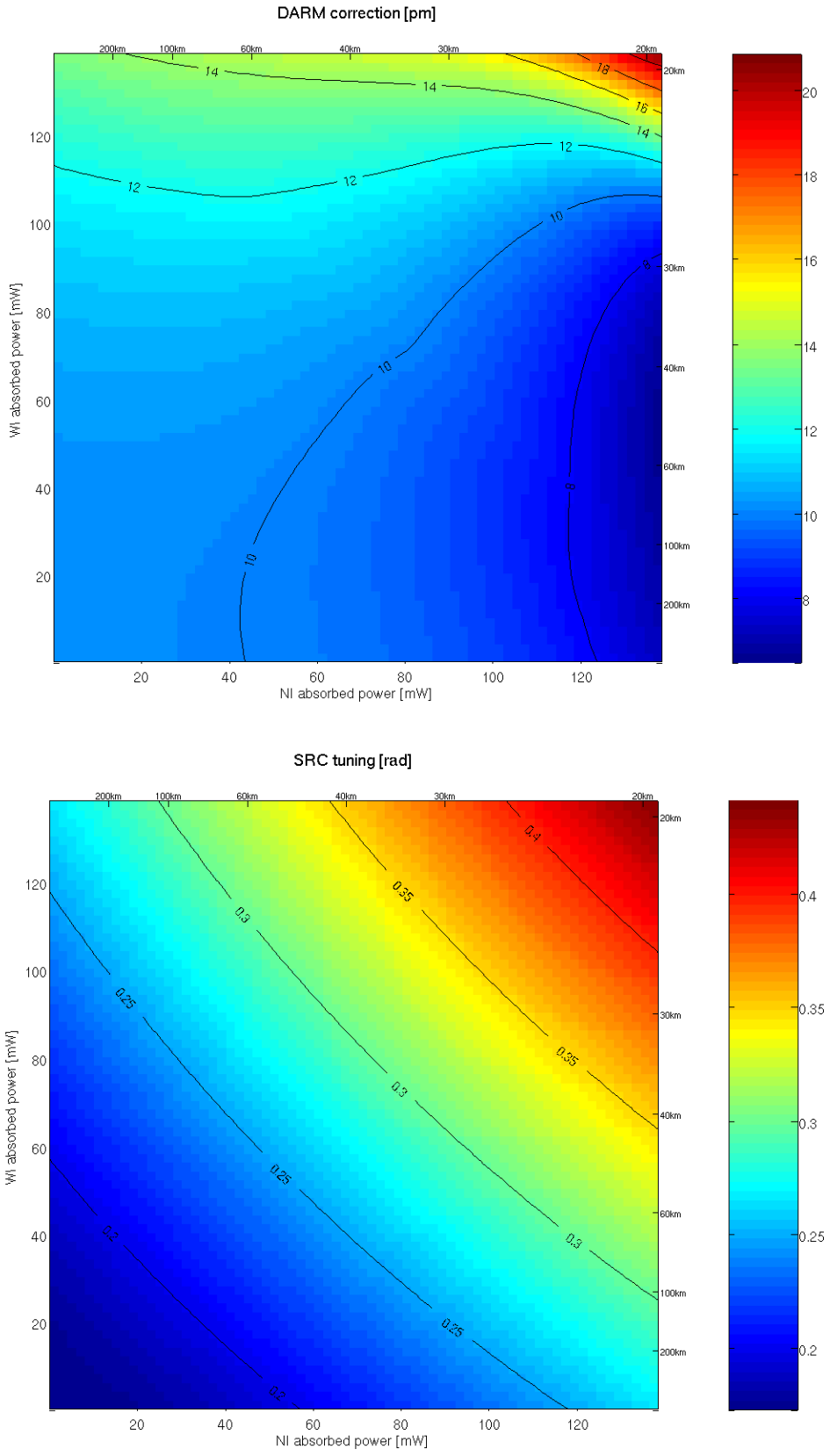


Figure 19: **MSRC.** DARM (top) and SRCL (bottom) corrections.

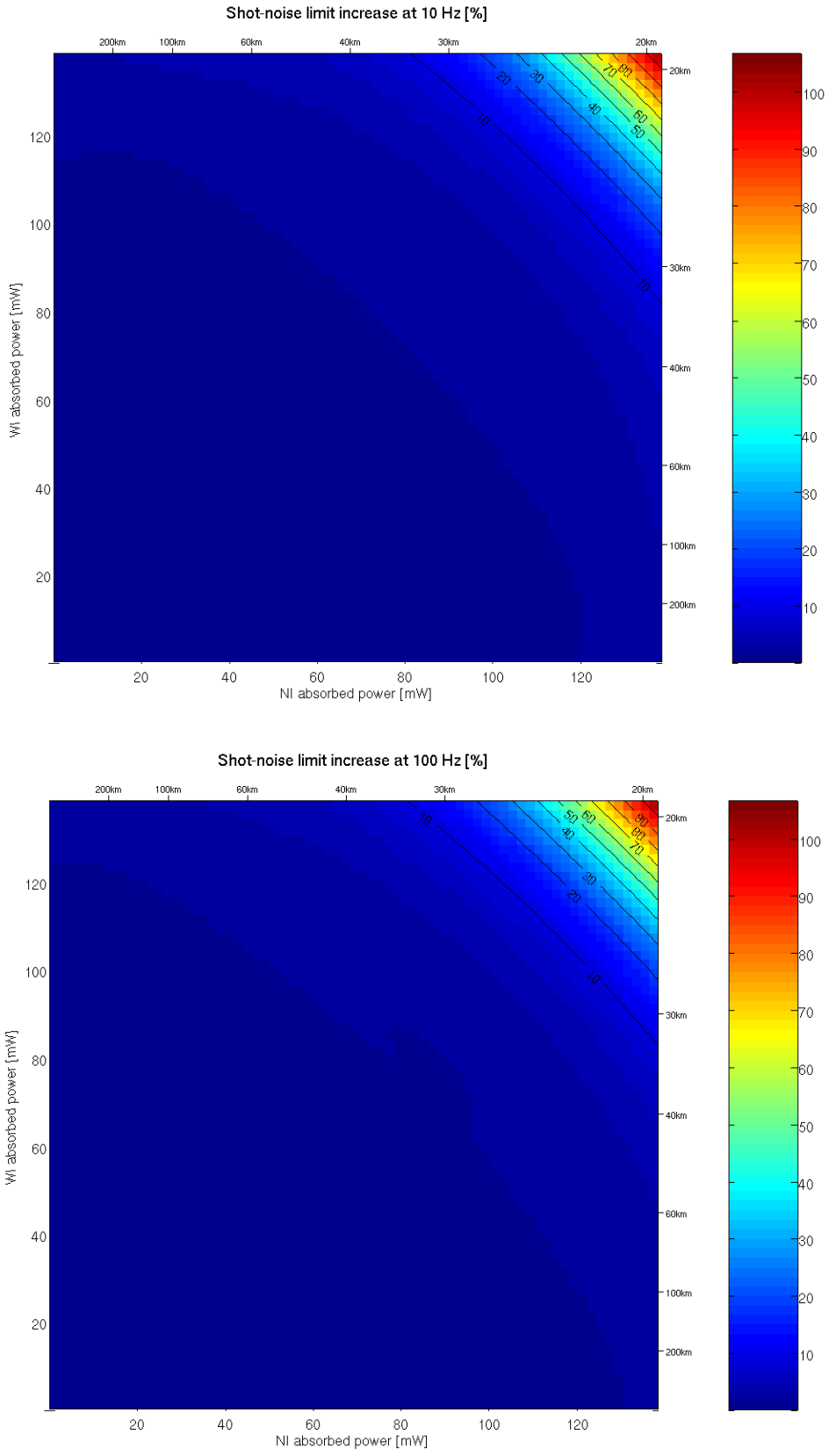


Figure 20: **MSRC.** Percentual worsening of shot-noise-limited sensitivity at 10 Hz (top) and 100 Hz (bottom).

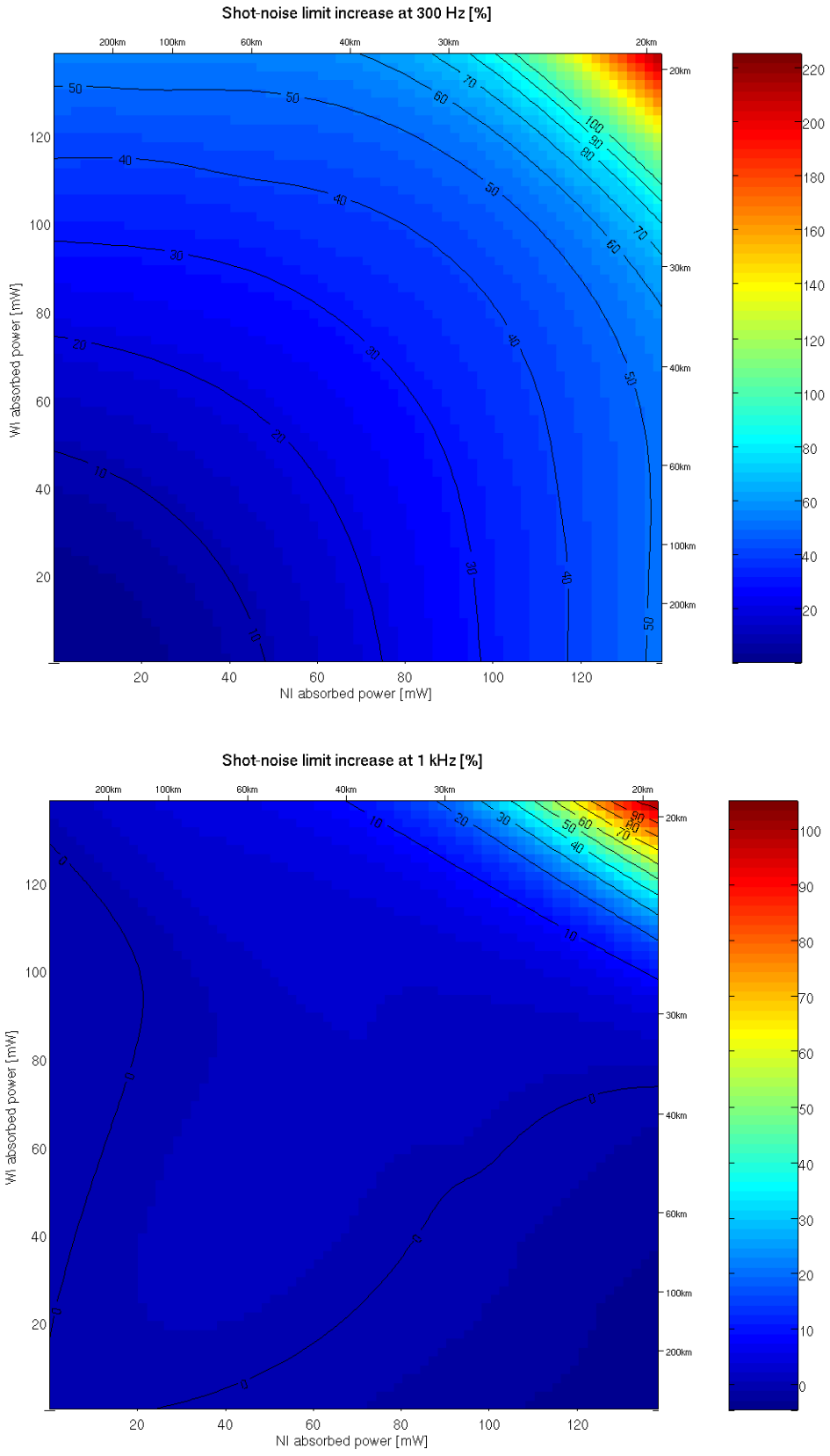


Figure 21: **MSRC.** Percentual worsening of shot-noise-limited sensitivity at 300 Hz (top) and 1000 Hz (bottom).

## 6.2 Non-Degenerate Recycling cavity

The simulation described here has been carried out without any astigmatism.

Carrier and sidebands recycling gains are shown in fig. 23. The dependence on the common lensing is well visible along the plot main diagonals and reproduce quite well the results explained in the previous sec. 5.1. The dip at the lensing that makes the $TEM_{04}$ mode resonant is visible also in this plot. Some small dependence on differential lensings is present, but in general the carrier recycling gain remains always reasonably good. The situation is much different considering the sideband recycling gain: along the diagonal the gain is always good, but differential lensings play a dramatic role: indeed NDRC cavities are quite vulnerable to differential thermal lensing. This topic is rather complex and it will be better explained with more simulation results in sec. 8.

Fig. 24 shows the power inside north arm and at dark port. Both are clearly affected by the structure coming from the $TEM_{04}$ mode resonance.

Fig. 25 shows PRCL and CARM corrections. PRCL correction is clearly strongly affected by differential lensing with a shape that somehow resembles the power distribution of the sidebands. CARM correction as expected follows closely PRCL one to recover the good resonant condition inside the PRC-arm double cavity.

Fig. 26 shows DARM and SRCL corrections. DARM is as expected dominated by differential lensings, but the correction is in general not very large. SRCL seems mostly sensitive to common lensing, but the correction is not very large nor showing predominant structures.

The evolution of the interferometer shot-noise-limited sensitivity is shown in fig. 27 and 28. Again what is plotted there is the percentual worsening of the sensitivity at the frequency:

$$z = 100 \times \frac{h_{thermal}(f) - h_{cold}(f)}{h_{cold}(f)}$$

The noise level around 10, 100 and 1000 Hz is almost constant, except for the well known $TEM_{04}$ resonant zone, where some 10% can be lost. The most significant effect is again visible around 300 Hz. As shown in the previous section 5.2 there is no effect along the common lensing diagonal, but the effect of differential lensings is rather large. It can make the sensitivity worsen by 20% with unbalanced residual lensings of for example 100 km and 30 km. The order of magnitude of this effect is comparable to the common mode one for MSRC. Some shot-noise curves are shown in fig. 22

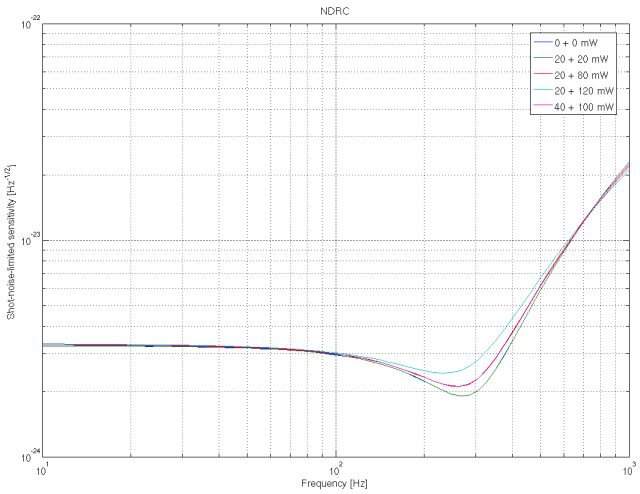


Figure 22: **NDRC.** Shot-noise-limited sensitivities for different combination of thermal lensing.

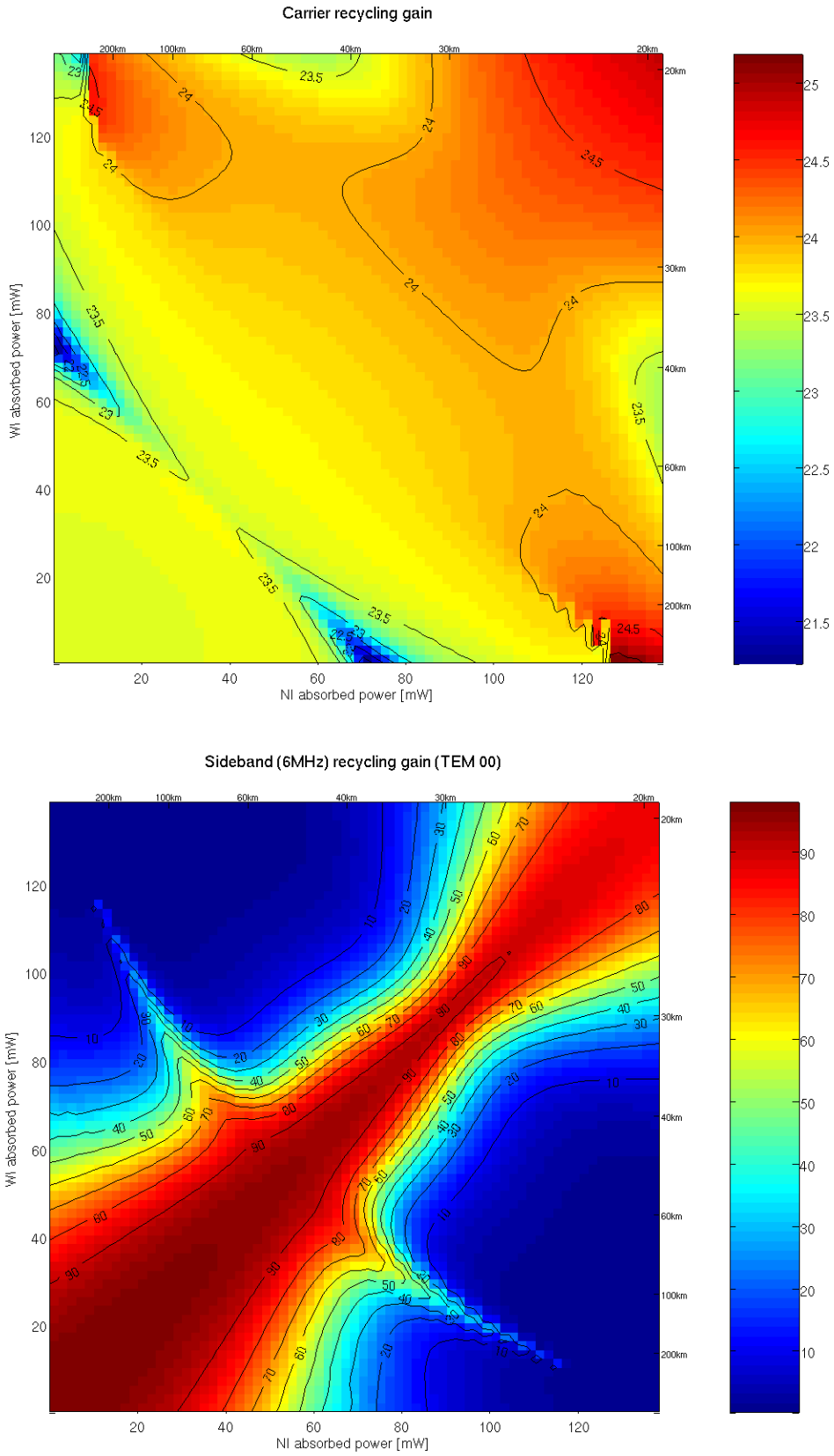


Figure 23: **NDRC.** Carrier (top) and sideband (bottom) recycling gain ($TEM_{00}$)

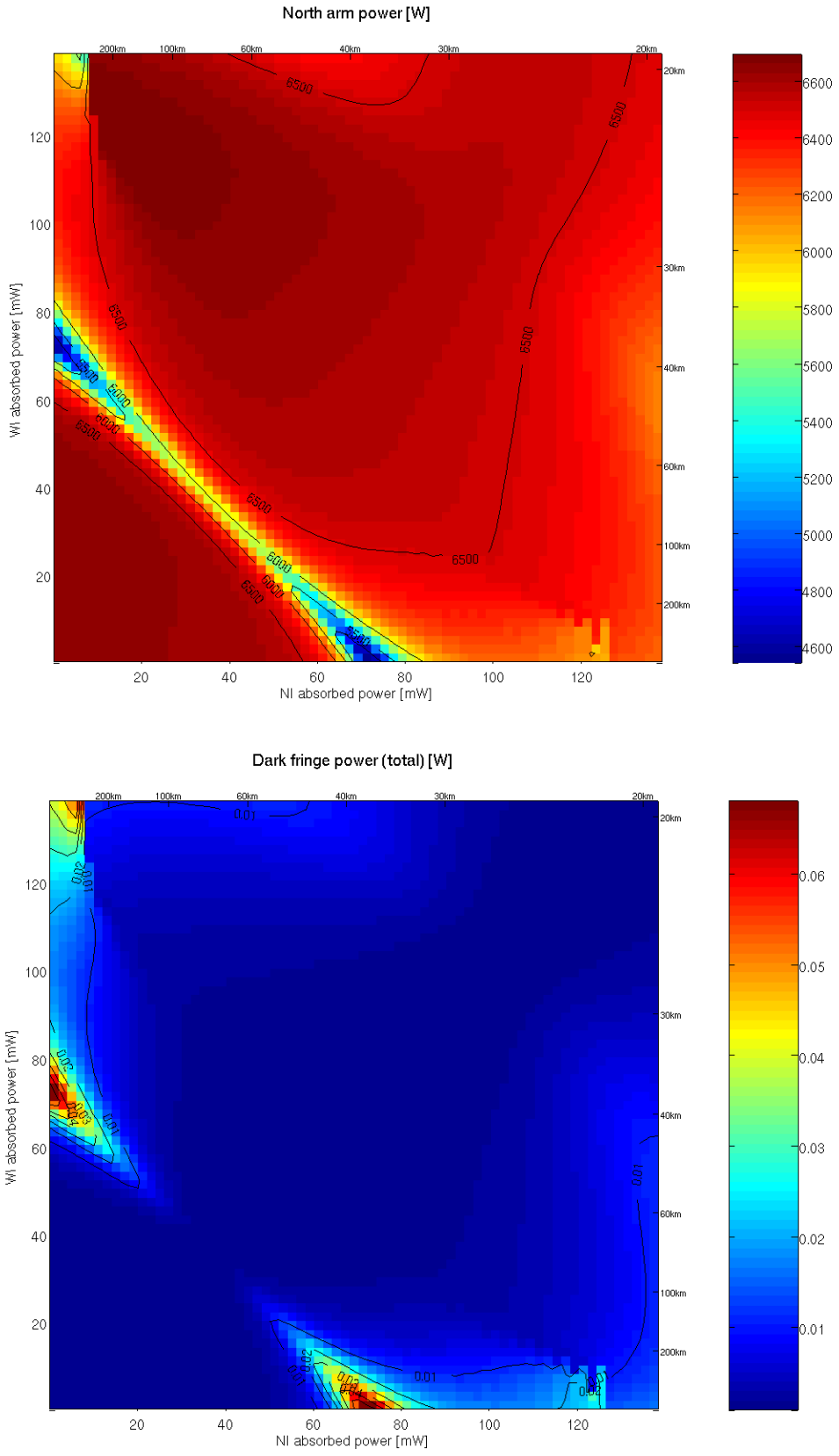


Figure 24: **NDRC.** Power inside north arm (top) and at dark port.

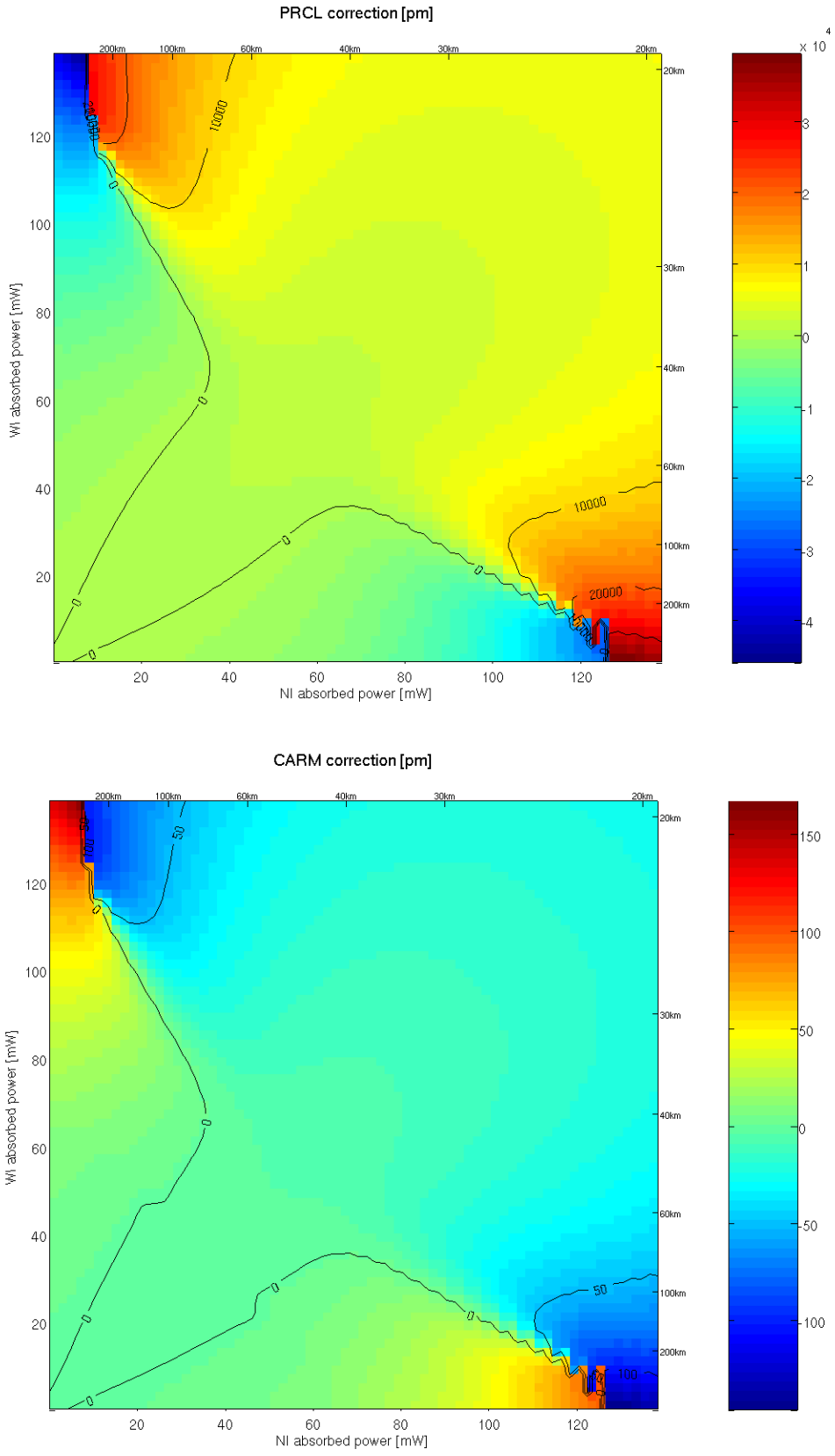


Figure 25: **NDRC.** PRCL (top) and CARM (bottom) corrections.

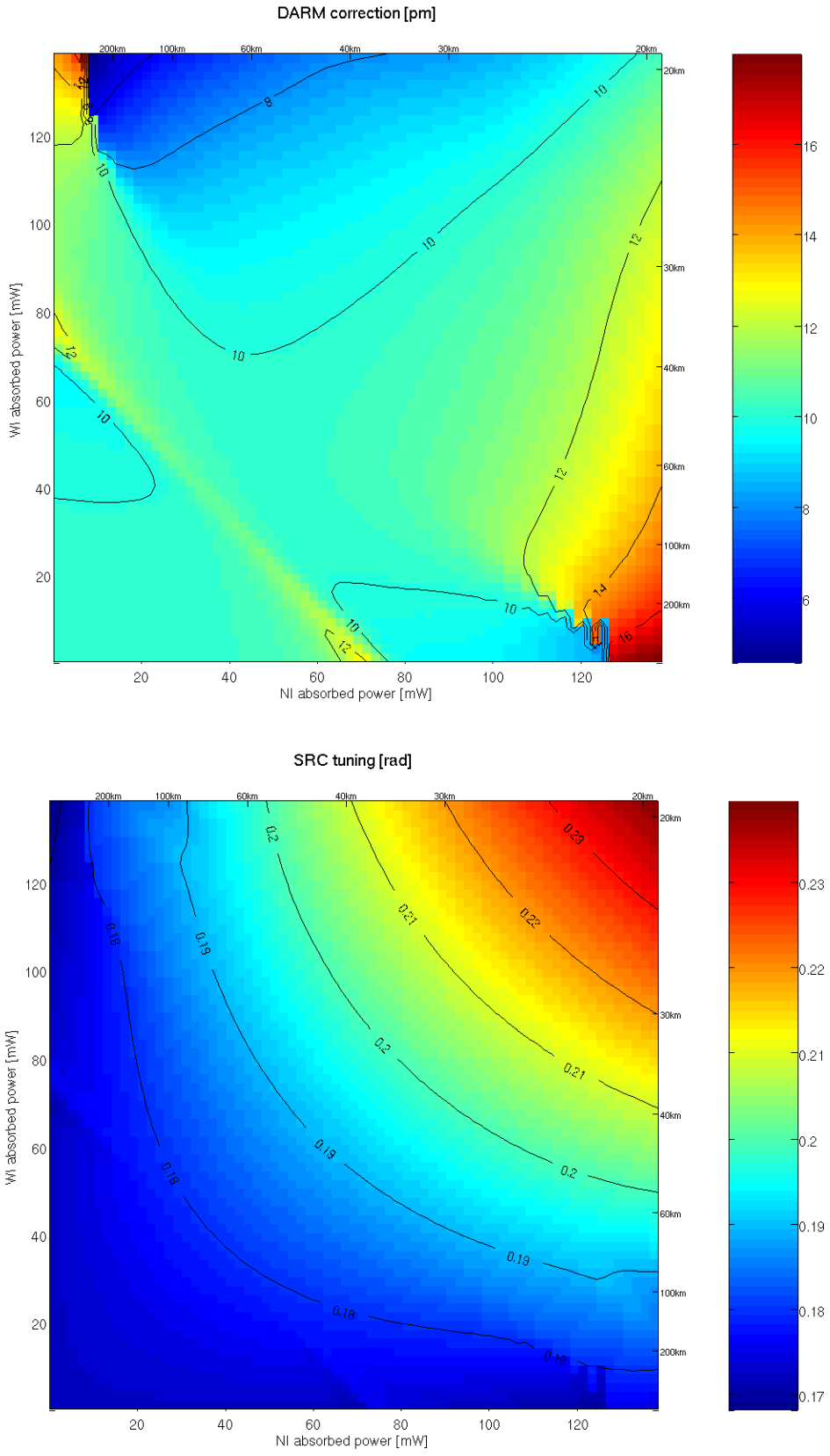


Figure 26: **NDRC.** DARM (top) and SRCL (bottom) corrections.

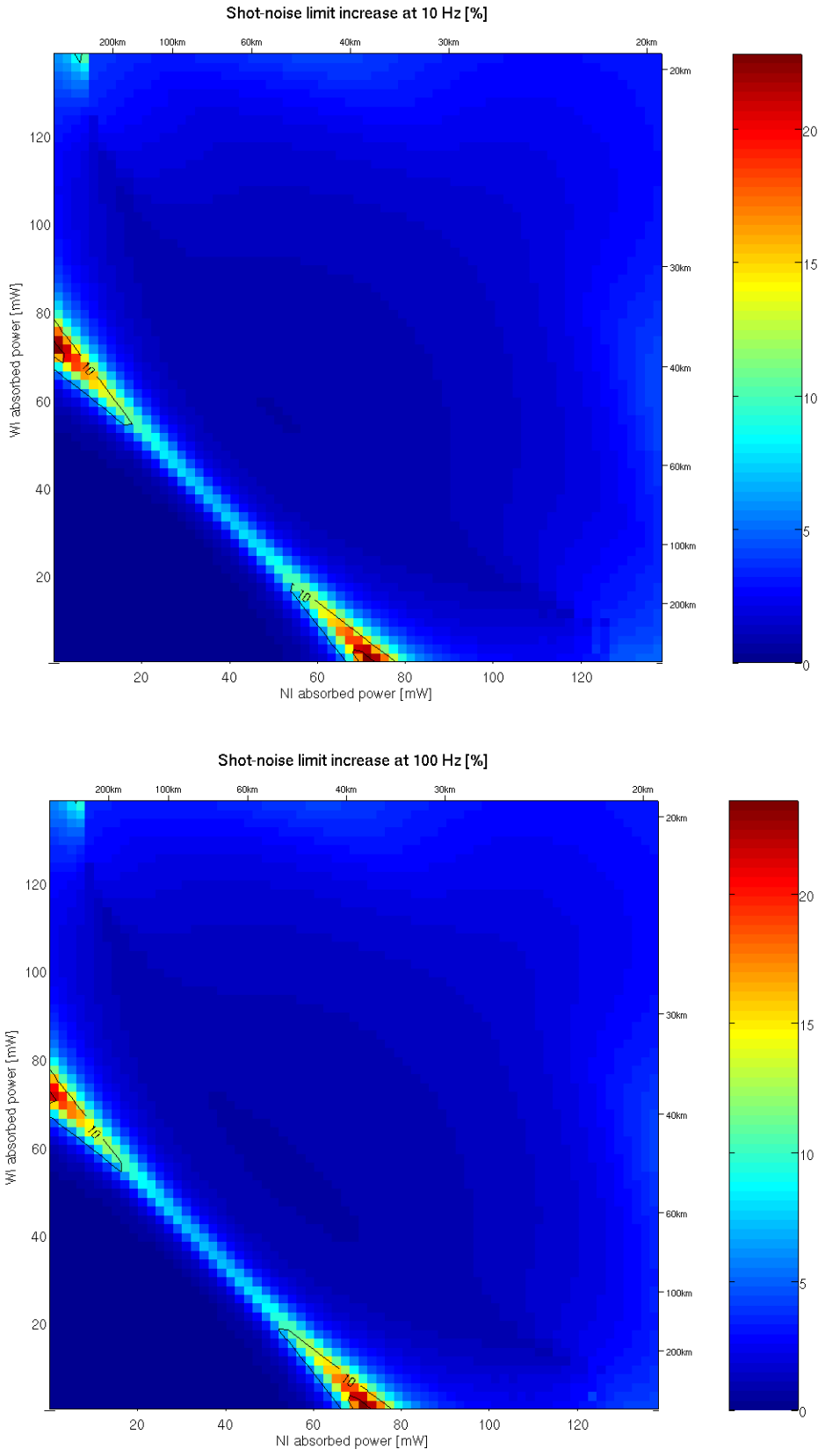


Figure 27: **NDRC.** Percentual worsening of shot-noise-limited sensitivity at 10 Hz (top) and 100 Hz (bottom).

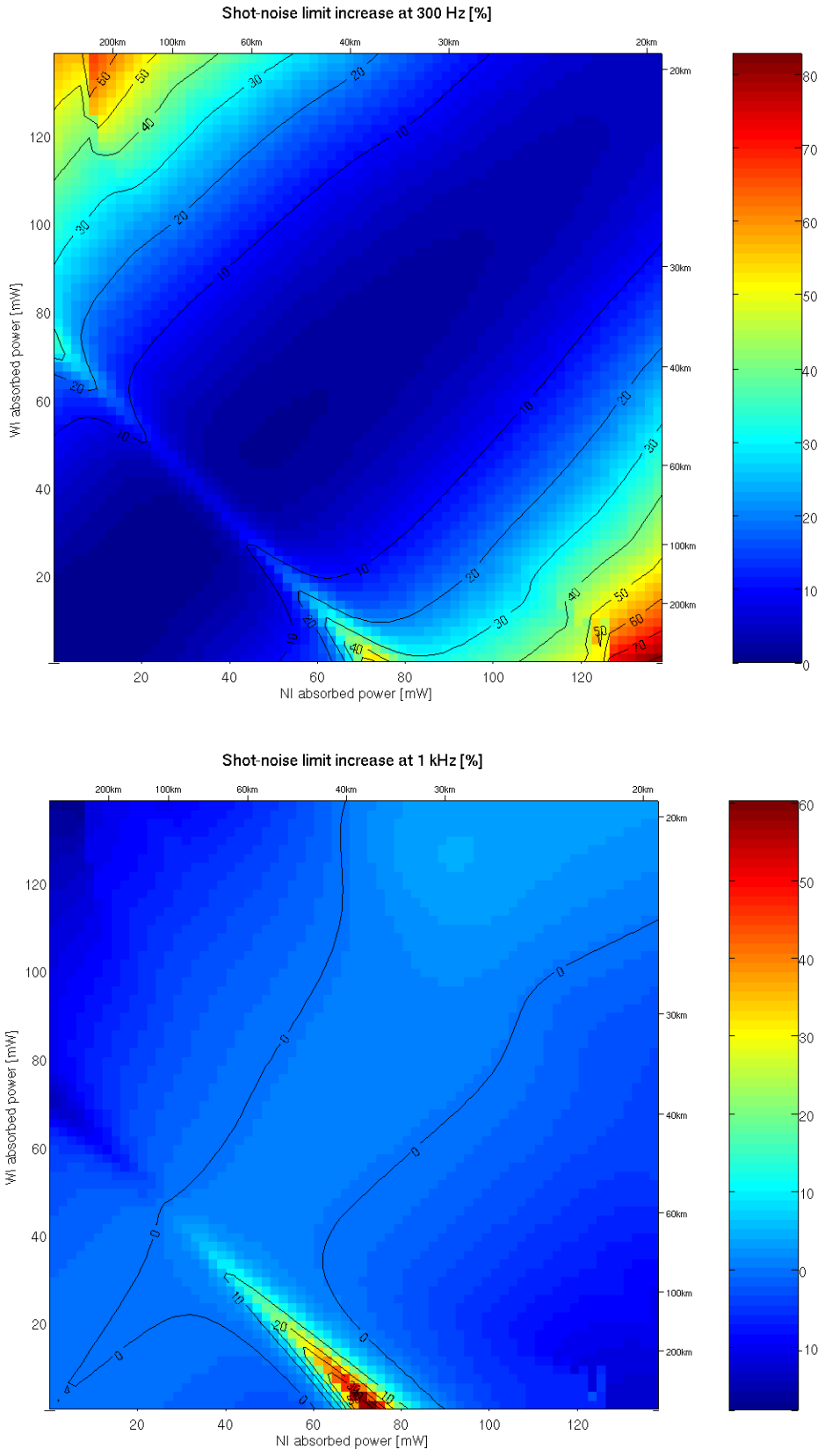


Figure 28: **NDRC.** Percentual worsening of shot-noise-limited sensitivity at 300 Hz (top) and 1000 Hz (bottom).

### 6.3 Discussion

The simulations reported in this section shows that in a dual recycled interferometer the response to common and differential lensings are quite different.

Common lensings affects mainly a marginally stable signal recycling cavity, resulting in a reduction of the shot-noise limited sensitivity around the frequency of peak sensitivity. This reduction is however, at least in the simulated case of de-tuned signal recycling, not dramatic and can be contained within 10% with not too stringent requirements on thermal compensation system performances. A non-degenerate signal recycling cavity is almost immune to common mode lensings.

On the other hands, marginally stable recycling cavities are completely immune to differential thermal lensings, while non-degenerate recycling cavities are strongly affected, both for what concerns radio-frequency sidebands and sensitivity. For the main RF sidebands the effect of differential thermal lensing can be quite large and dependent also on the common mode. The investigation of this effect is the topic of the sec 8. Concerning the sensitivity the loss can be of the same order of magnitude as for the MSRC with relatively small unbalanced lensings.

## 7 Simulation of astigmatism in NDRC

### 7.1 Astigmatism without thermal effect

So far NDRC were simulated simply enforcing an ad-hoc Gouy phase in propagation, thus without a proper model of the real folding telescope. To take into account the effect of astigmatism, a full model is needed. The parameters used here are those listed in 3, which refers to the so-called 2bis configuration: two recycling mirrors are suspended from the injection or detection bench and the third one from the beam splitter. This is the only configuration which allows to reduce the incidence angle to relatively small values (1.34 degrees). The first modulation frequency has been tuned to be anti-resonant in the arms and resonant in PRC. This required a small adjustment (few cm) of $L_1$. The modulation that corresponds to this optical design is not really possible, since it implies an input mode cleaner almost 150 m long. However the main results are not affected by this choice.

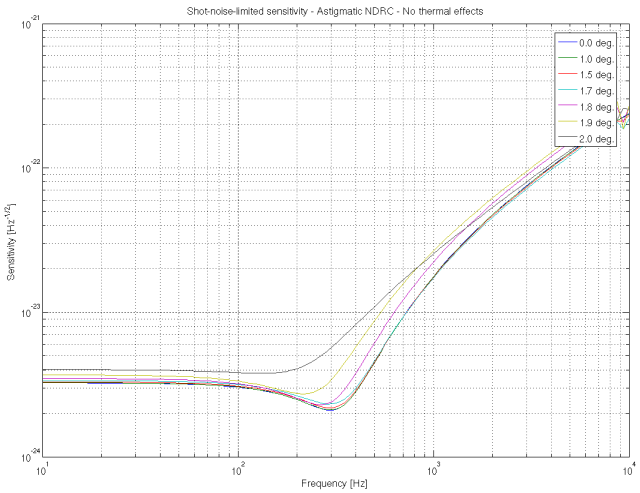


Figure 29: Dependence of the optimized shot-noise-limited sensitivity on the incidence angle of beams in the signal recycling non-degenerate folded cavity.

Fig. 29 shows how the astigmatism introduced by the non null incidence angle on the NDRC curved mirrors is quite important for determining the maximum achievable sensitivity. To obtain these results the same radii of curvature and lengths were maintained, but the angle was changed. The results shows clearly that to avoid loosing more than 10% in peak sensitivity the angle must be smaller than 1.5 degrees. With 1 degree there is no significant difference with respect to the non-astigmatic case. It is important to stress that this simulation was performed without any thermal effect: the entire interferometer was perfect except for the astigmatism.

The difference with respect to the case of a defect like a thermal lensing is striking. Indeed, a thermal lens in the NDRC signal recycling cavity is compensated by the locking algorithm shifting a bit the SRC tuning. Astigmatism can be viewed as a non-axis-symmetric lensing: therefore the SRC re-tuning can compensate only part of it and therefore there is a residual worsening of the sensitivity.

For completeness the following table reports carrier and sidebands recycling gains for the $TEM_{00}$ mode with few different incidence angles:

| **Angle [deg.]** | **Carrier** | **Sidebands** |
|---|---|---|
| 0.0 | 23.54 | 96.76 |
| 1.0 | 23.53 | 96.76 |
| 1.5 | 23.36 | 88.97 |
| 1.7 | 22.76 | 74.14 |

## 7.2 Astigmatism with thermal effects

The same thermal lensing map simulated without astigmatism has been reproduced with the full model of the non-degenerate recycling cavities. The differential effect has a different behavior, since the signal recycling cavity length has been changed with respect to the previous simulation. The reason of this change will be explained in sec. 8. This implies some difference in the correction signals. The sensitivity behavior is quite similar except for the appearance in the 10 and 100 Hz regions of a structure along the cross diagonal, related to high order modes resonances. Also the behavior of the high frequency band is changed, but the effect on the sensitivity is not huge. In the most relevant band around 300 Hz the behavior with or without astigmatism is similar.

The structure around the cross-diagonal are related, as explained in sec. 5.1, to fourth order modes becoming resonant inside the power recycling cavity. Astigmatism split the three $TEM_{04}$, $TEM_{22}$ and $TEM_{04}$ modes, which are resonant for different combinations of lensings (see fig. 36).

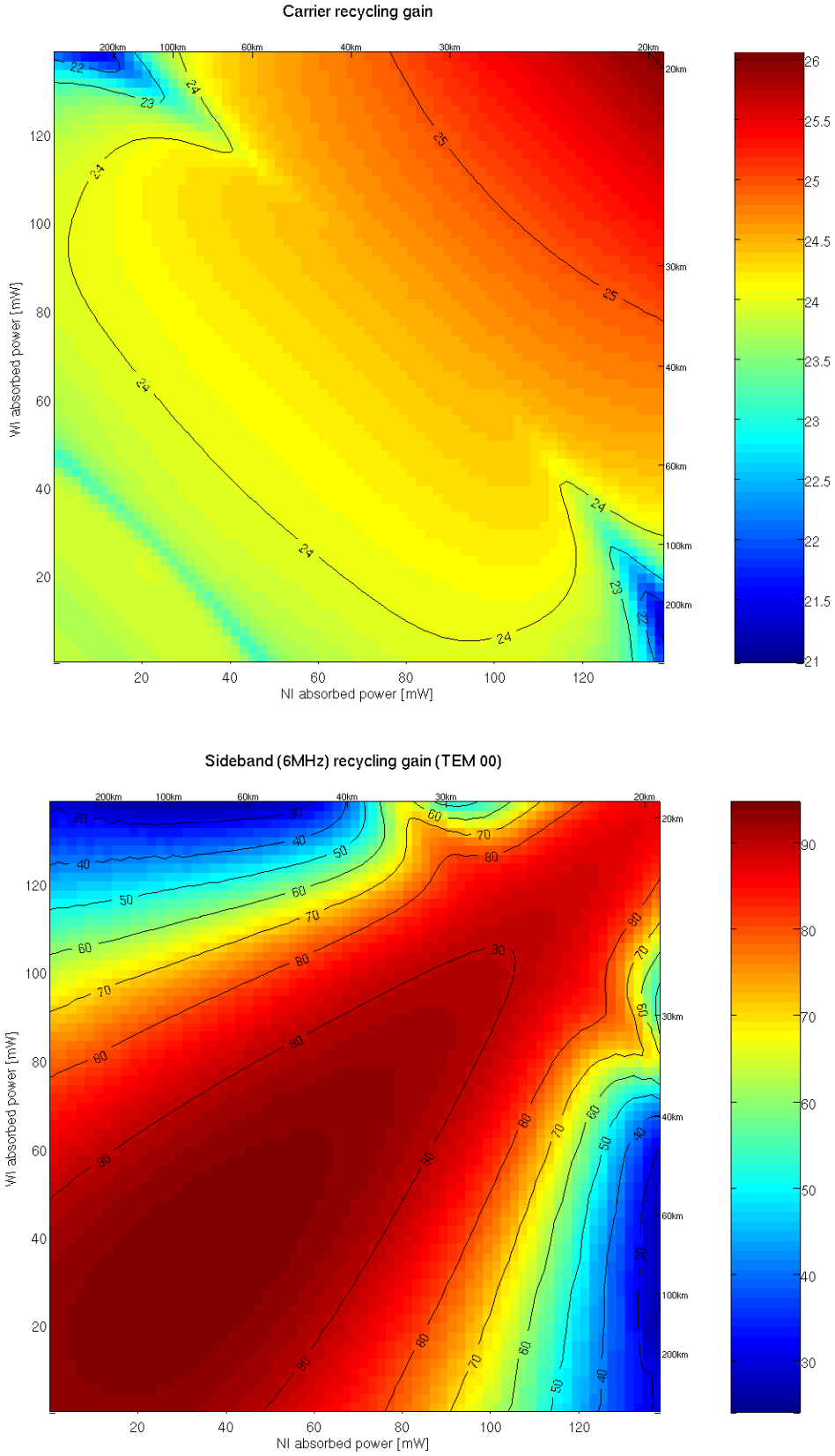


Figure 30: **NDRC with astigmatism.** Carrier (top) and sideband (bottom) recycling gain ($TEM_{00}$)

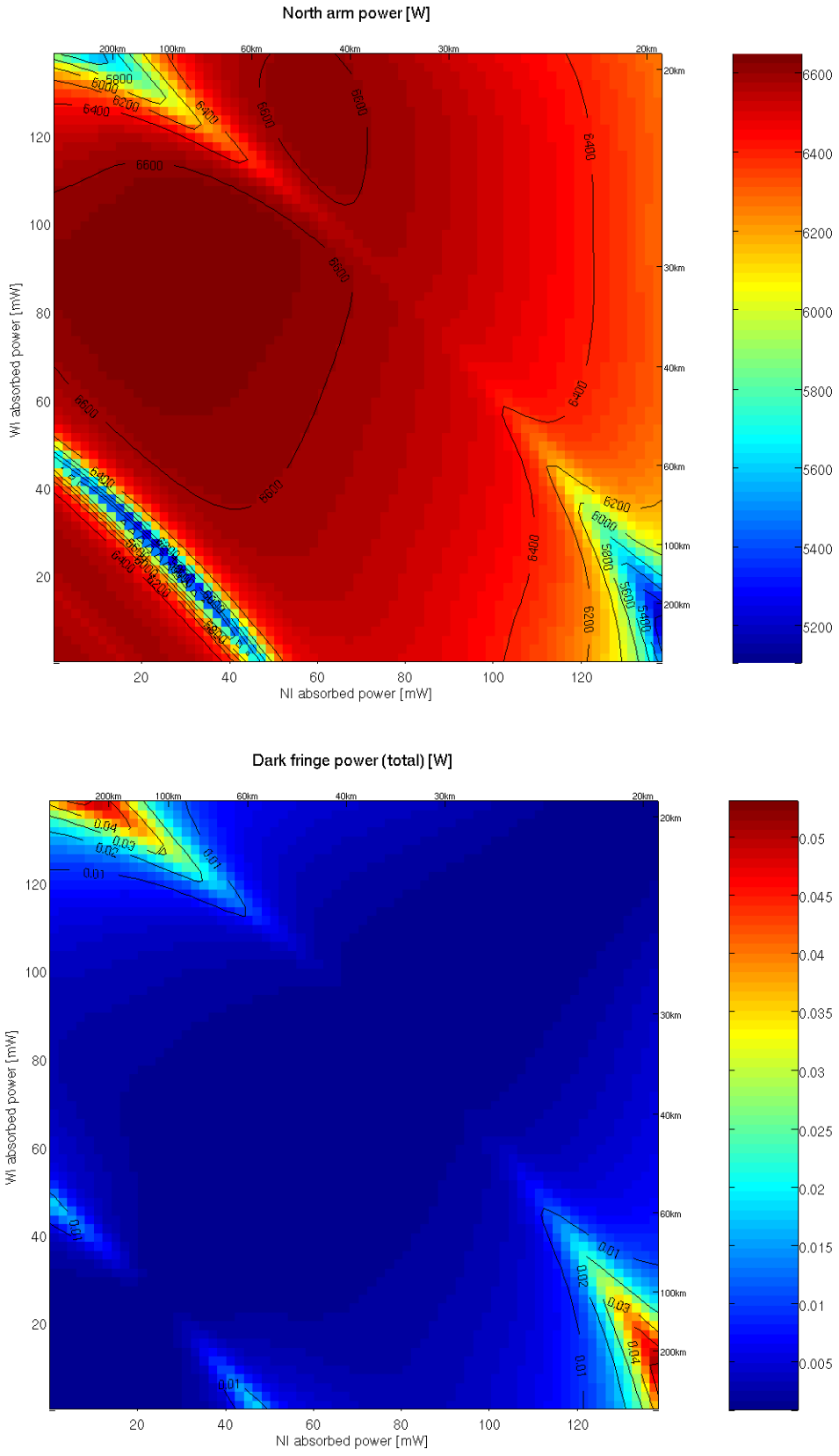


Figure 31: **NDRC with astigmatism.** Power inside north arm (top) and at dark port.

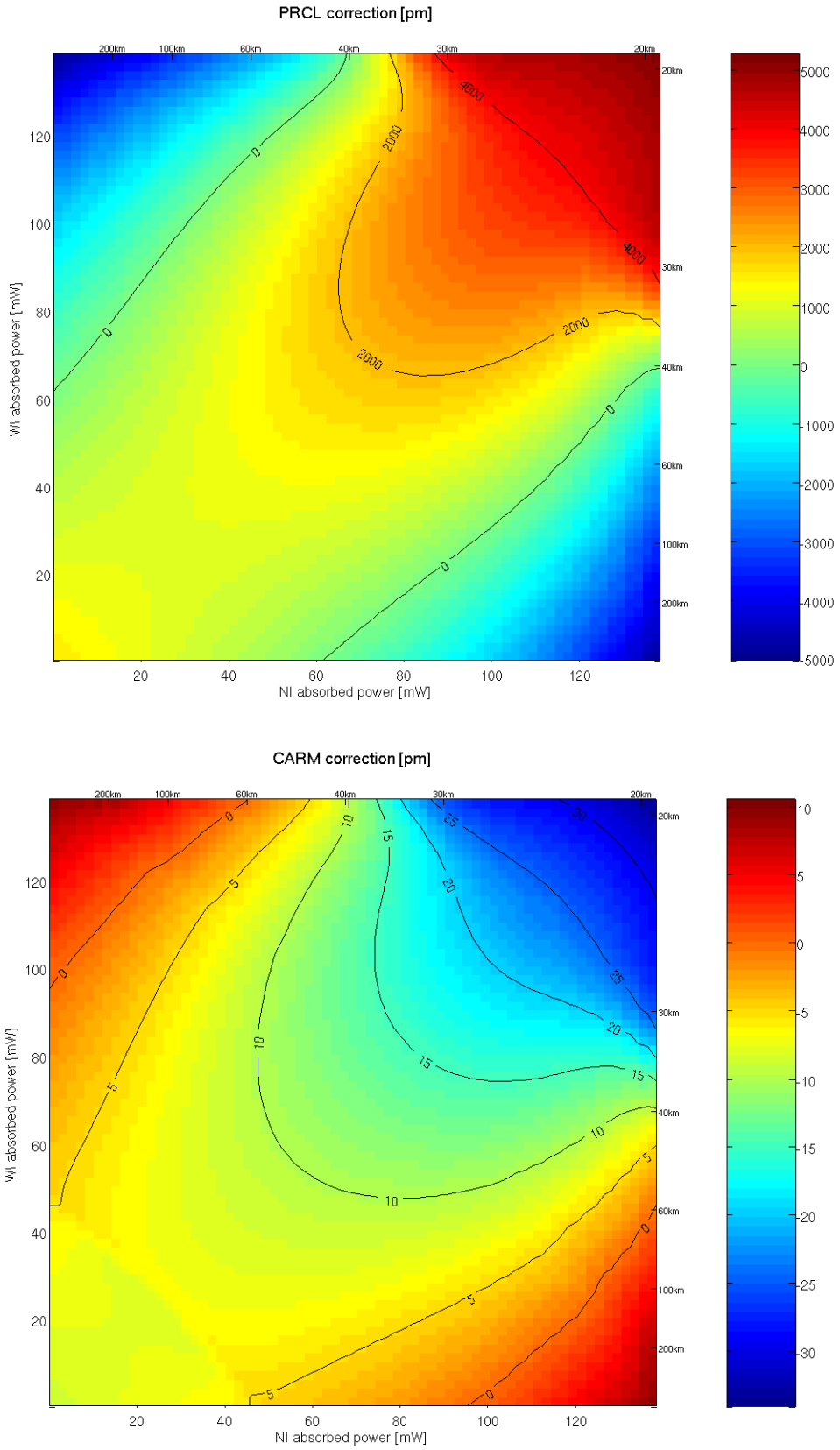


Figure 32: **NDRC with astigmatism.** PRCL (top) and CARM (bottom) corrections.

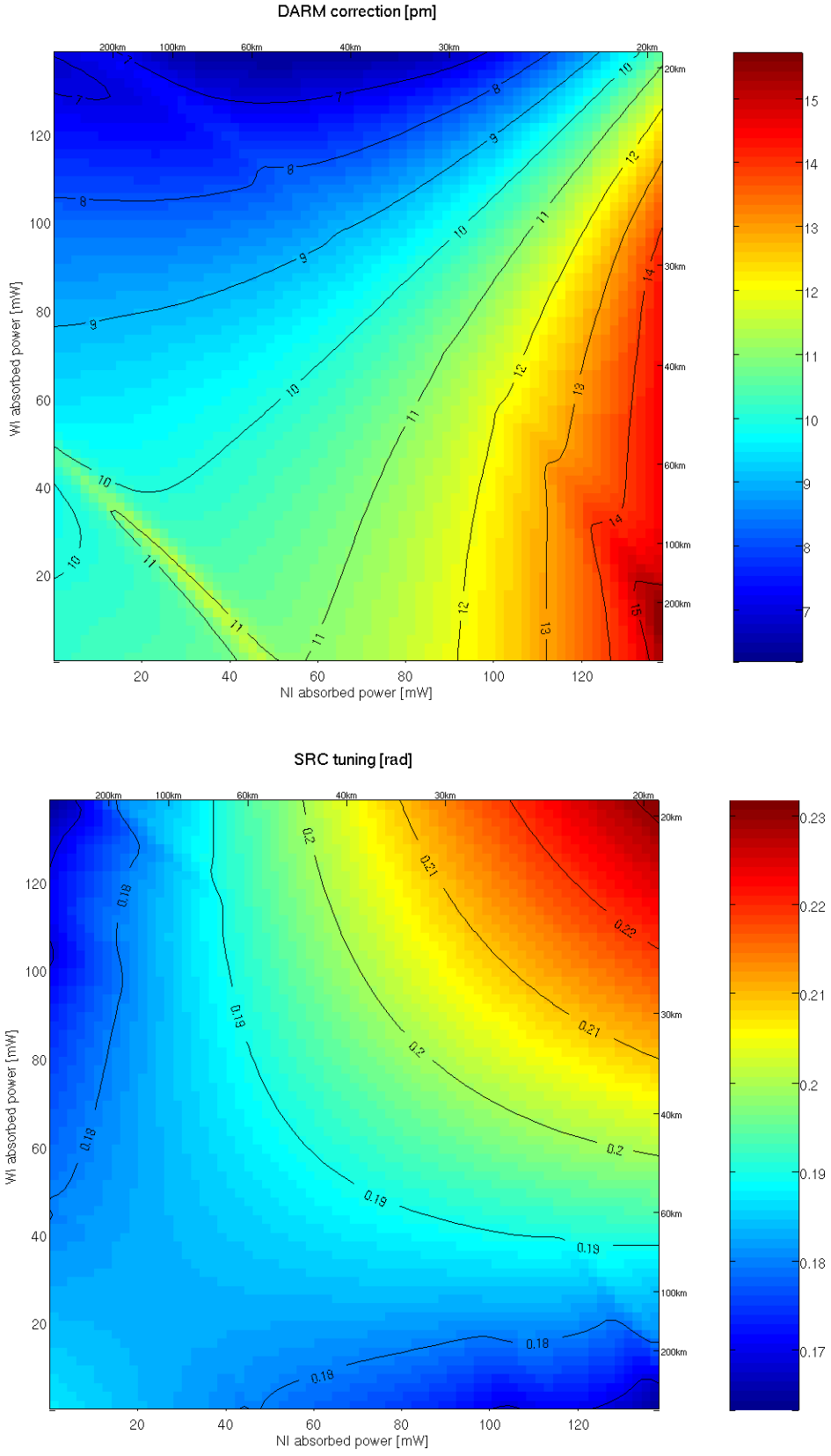


Figure 33: **NDRC with astigmatism.** DARM (top) and SRCL (bottom) corrections.

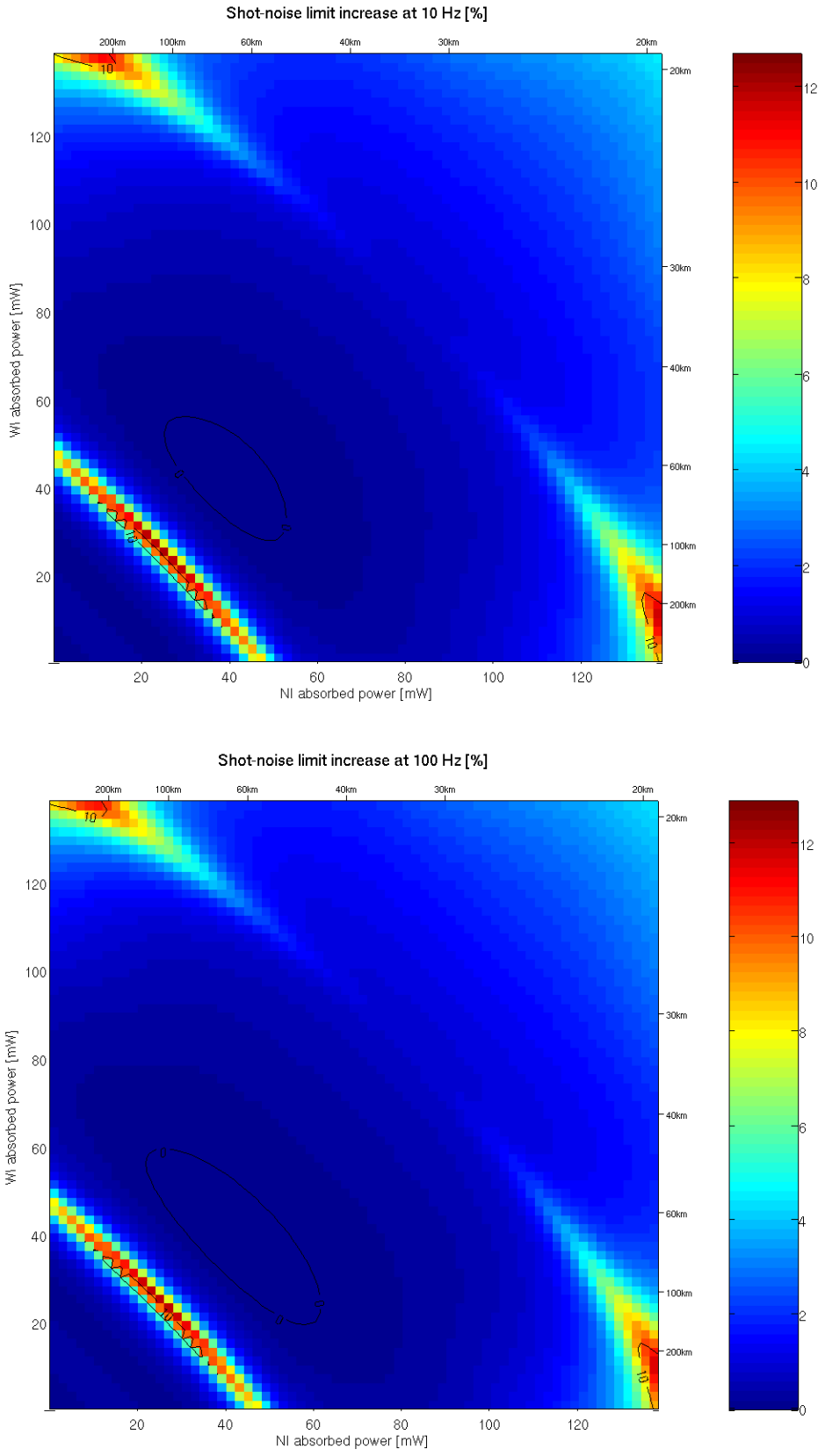


Figure 34: **NDRC with astigmatism.** Percentual worsening of shot-noise-limited sensitivity at 10 Hz (top) and 100 Hz (bottom).

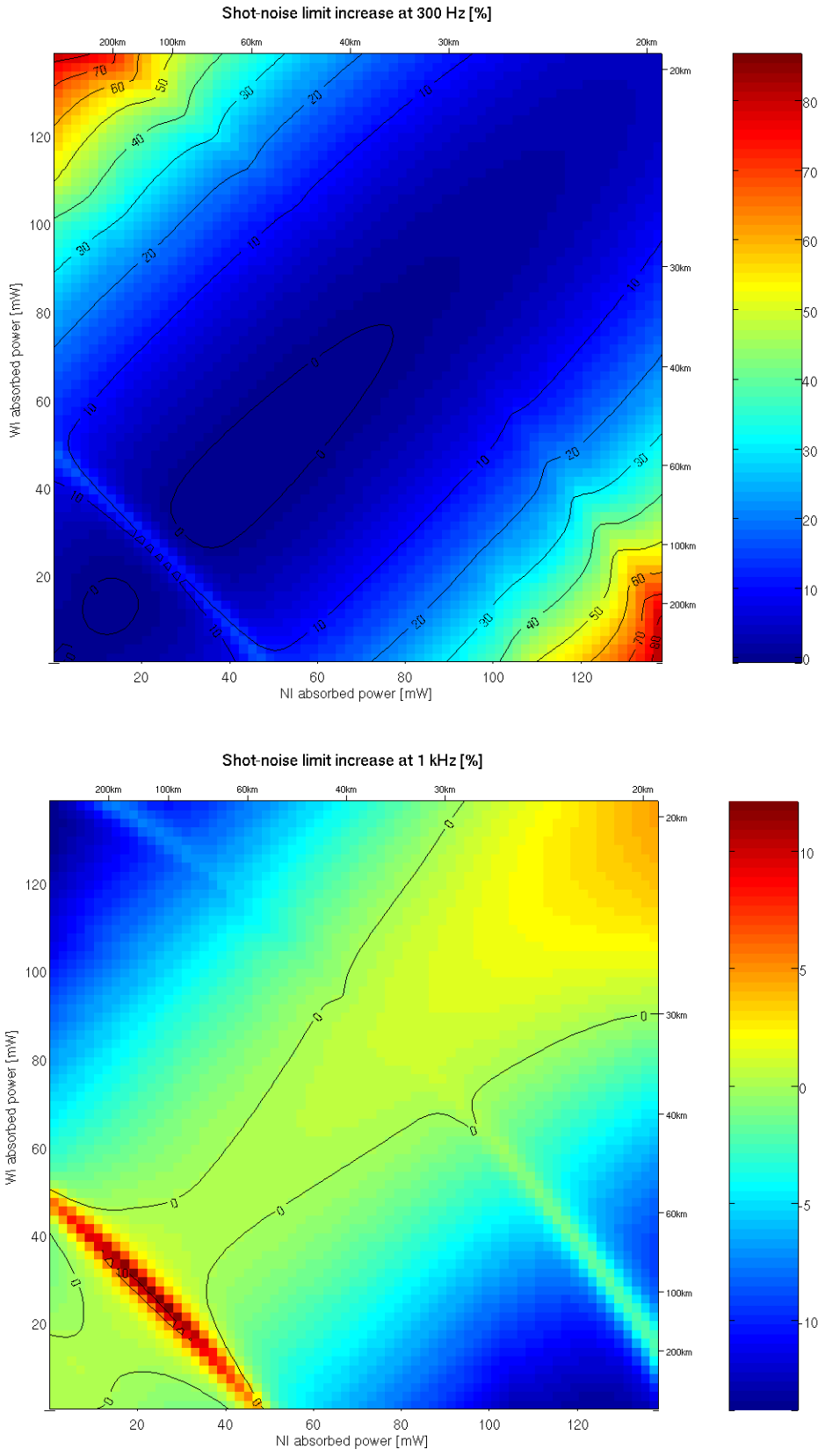


Figure 35: **NDRC with astigmatism.** Percentual worsening of shot-noise-limited sensitivity at 300 Hz (top) and 1000 Hz (bottom).

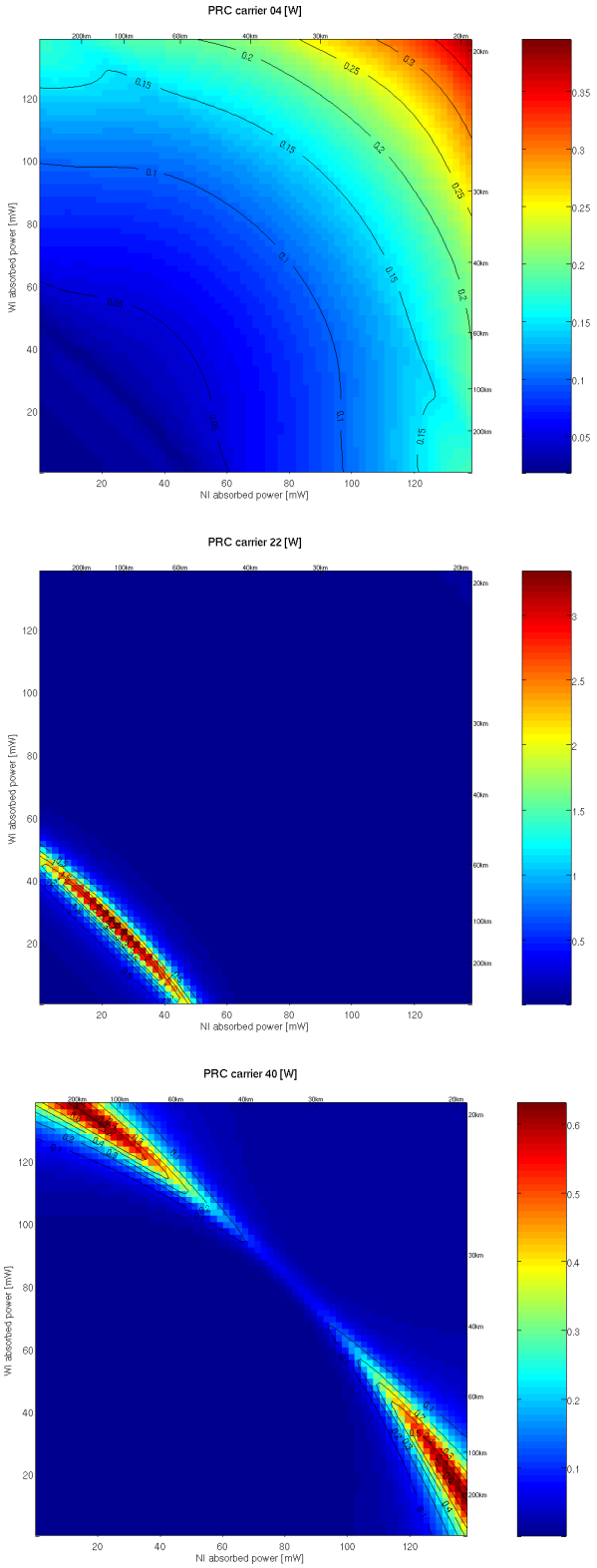


Figure 36: **NDRC with astigmatism.** Resonance condition of fourth order modes inside PRC.

# 8 Effect of differential thermal lensing

## 8.1 Non-Degenerate Recycling Cavity

As already explained in previous sections, one of the main weakness of the non-degenerate recycling cavity is the sensitivity to differential thermal effects. This effect is peculiar of the dual-recycled interferometer: indeed the simulation shows that removing the signal recycling cavity removes this effect. It is moreover independent of the Schnupp asymmetry (the effect is there even with null asymmetry) but it depends on the Gouy phase chosen for propagation inside the signal recycling cavity and on the length of the SRC. Fig. 37 shows the effect on sideband recycling gain for different choices of SRC Gouy phases. A mean value for the two input mirror absorption is set to 100 mW and the individual values are changed differentially. There is a clear dependence on the Gouy phase but without an evident regularity.

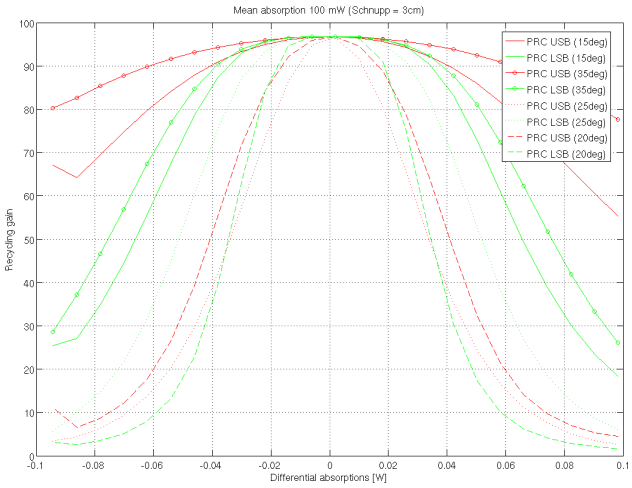


Figure 37: **NDRC.** Sideband recycling gain (power inside PRC) as a function of differential thermal lensing, for different choices of SRC Gouy phase.

Fig. 38 shows the result of a simulation in which the signal recycling cavity length is fixed as well as the Gouy phase but the SRC tuning is changed. Here the two cavities are not astigmatic and a small pure differential thermal lensing is applied, corresponding to about 100 km and -100 km of focal lengths. The upper and lower sidebands show two large drops in recycling gain in correspondence of the signal recycling tunings that make the second order higher mode resonant inside SRC. The effect can be quite easily understood: a differential lensing will create high order modes inside the two short Michelson arms with opposite signs. Because of the dark fringe locking condition, this differential high order mode is not transmitted to PRC but it is perfectly coupled to SRC. If the mode becomes resonant therein, the SRC transmission for this mode increases and the neat result is a large subtraction of power from the fundamental mode of the PRC. In other words, in presence of differential lensings the fundamental mode inside PRC sees an additional output port toward SRC due to differential high order modes. If the SRC becomes resonant, the transmission of this output port is largely increased. Even if only few percent of $TEM_{00}$ power is lost through high order modes inside SRC, this has to be compared with the power recycling transmission which is also of the order of few percents.

The position of the upper and lower sideband gain dips is consistent with the resonance of second order modes. At zero tuning the carrier is anti-resonant in SRC. The first sideband frequency is not well tuned to the signal recycling cavity length, therefore the upper and lower will get an additional dephasing of 120 degrees which makes then resonant inside SRC at 120 and 240 degrees, see again fig. 38. The Gouy phase in a single propagation in the SRC is 20 degrees, therefore the second order modes will resonate at about 40 and 160 degrees. These are exactly the tunings that destroy the PRC sideband recycling gains.

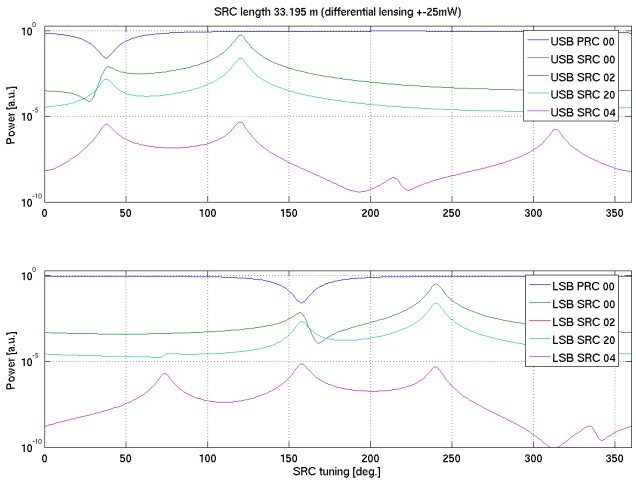


Figure 38: **NDRC.** Sideband power inside PRC in the fundamental $TEM_{00}$ mode and powers of high order modes inside SRC. Powers are normalized and therefore are in arbitrary units.

If astigmatism is introduced, the Gouy phase for the $TEM_{02}$ and $TEM_{20}$ modes is different and therefore they will resonate in different position. There will be four different regions of SRC tunings that make the PRC sideband power drop.

If the Gouy phase and the SRC tuning is fixed, the effect of changing the signal recycling length gives similar results. Fig. 39 shows the effect of changing the SRC length when single mirror thermal lensing is present: the NI mirror is perfect while a varying lensing is applied to the WI. There are four regions of lengths which are forbidden, corresponding to the $TEM_{02}$ and $TEM_{20}$ modes of USB and LSB becoming resonant inside SRC. As already explained the position of these regions depends on the SRC tuning and on the Gouy phase. It is interesting to notice how the effect is not negligible even for rather large residual thermal focal lengths, like 100 km.

A similar effect is also present for any other defect in the interferometer that creates differential high order modes. For example small mis-alignment can introduce loss of sidebands recycling gains in correspondence of the first order mode resonances. See for example fig. 40 where the two input mirrors have been mis-aligned of 25 nrad in one direction and very small thermal lensing have been introduces (corresponding to 10 and 6 mW absorbed power).

## 8.2 Marginally Stable Recycling Cavity

In the case of marginally stable recycling cavities the large sensitivity to differential lensing is not present. Fig. 41 compares the response of MSRC and NDRC with similar differential thermal effects, the nominal 0.15 rad SRC tuning, as a function of SRC length. The reason of the lower sensitivity is tracked to the degeneration of the cavity. The signal recycling cavity length is close to the power recycling one, therefore the sideband fundamental mode is close to anti-resonance in SRC. In the MSRC case, also all high order modes are in the same resonant condition of the fundamental one: therefore there is only one region where high order modes become all together resonant, but this is close to the carrier resonance, which is not an interesting region of SRC tunings.

## 8.3 Discussion

Differential thermal effects are a clear weak point of non-degenerate signal recycling cavity and they must be taken care in the design. Once the input mode cleaner length is fixed, the first sideband frequency is also

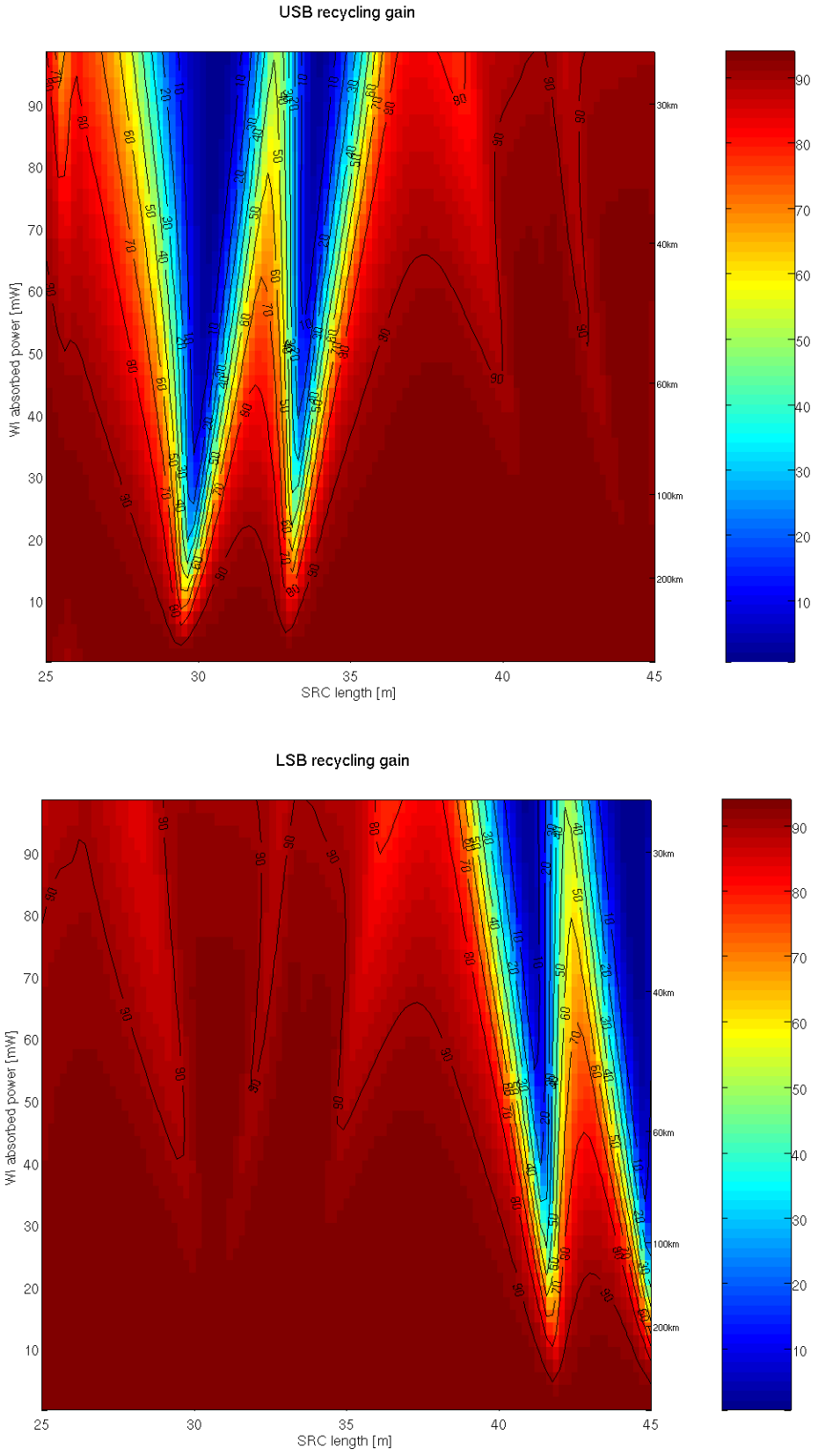


Figure 39: **NDRC.** Sideband power inside PRC in the fundamental $TEM_{00}$ mode for the upper (top) and lower (bottom) sidebands, as a function of the signal recycling cavity length and of a single mirror thermal lensing.

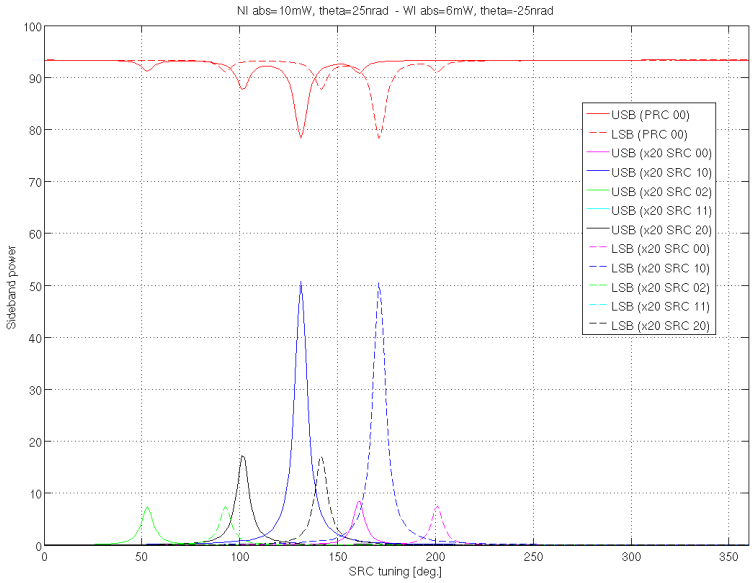


Figure 40: Effect of misalignments in sideband recycling gain loss.

almost fixed by it and the small possible range of PRC length. Afterwards the second modulation frequency must be a multiple of the first one and the SRC length must be chosen to make it resonant inside SRC: given the constraints from infrastructure, the choice might not be large. Once the Gouy phase of SRC telescope is selected, the analysis described in the previous sections must be repeated. One should take care that high order modes of USB and LSB (both even and odd modes) do not resonate close to the desired SRC tuning. In general, if only modes of relatively low order can be considered ($m + n \leq 6$ for example) and the Gouy phase can be taken to be small enough (for example 20 degrees as in the baseline) then the region of forbidden SRC tunings stays only on one side of the zero. Since the sensitivity is the same for positive and negative tunings, there should always be a relative large workable region around the needed tuning.

Even if a workable design might be feasible, there remain the problem of SRC lock acquisition. It is likely that during the acquisition of signal recycling mirror control, the SRC tuning will be far from the final one. In presence of small residual thermal lensing or misalignments, when SRC tuning crosses a first or second order sideband mode resonance, one of the main sideband $TEM_{00}$ powers inside PRC will drop, spoiling all longitudinal error signals.

This problem is much mitigated in the case of marginally stable signal recycling, since only one region around carrier resonance is forbidden, independently of thermal effects of residual misalignments.

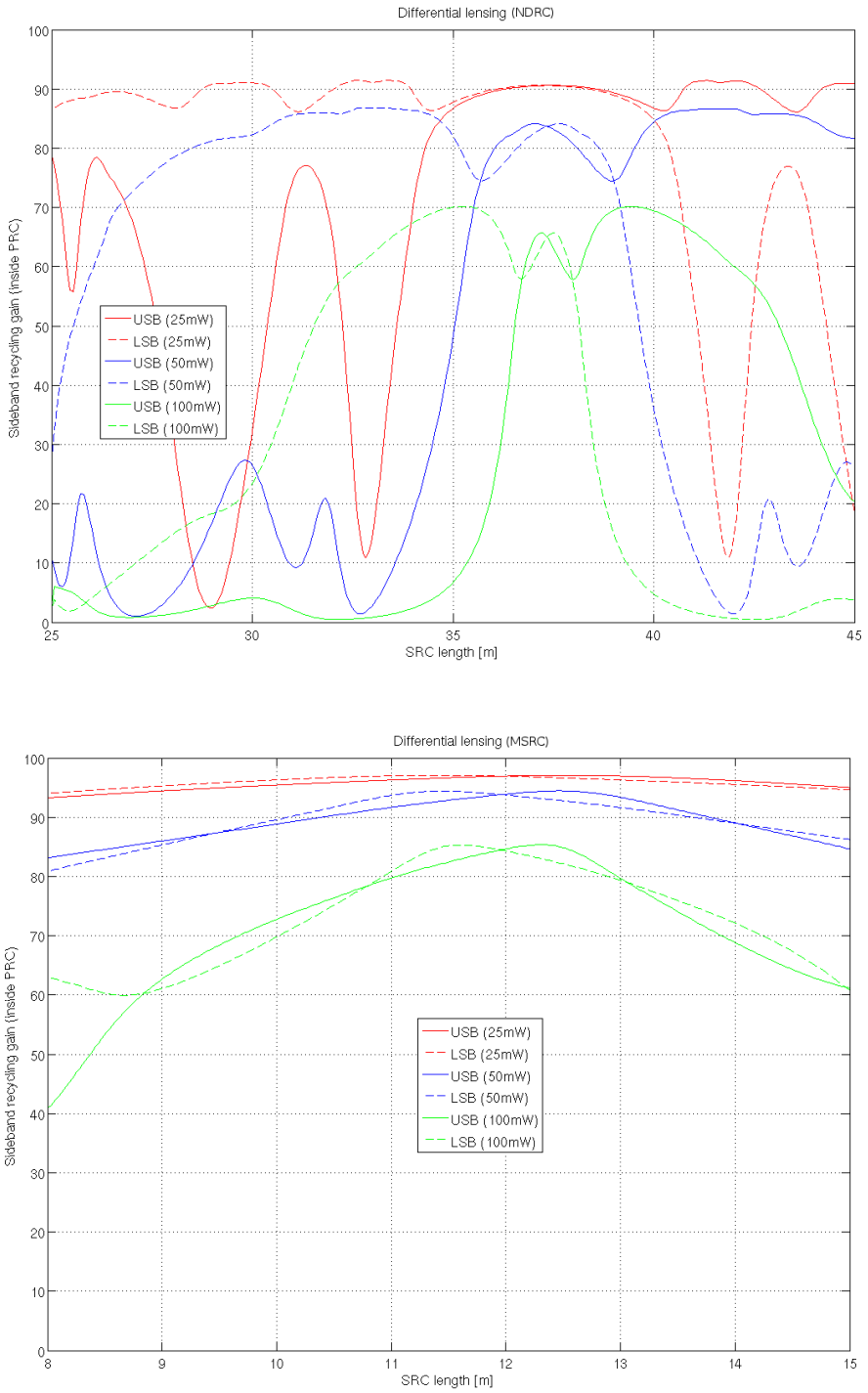


Figure 41: Comparison of sensitivity to differential lensings in MSRC and NDRC configuration.

# 9 Simulation with TCS phase maps

So far all thermal effects have been simulated in terms of simple spherical lenses. However in presence of thermal effects in the input mirror plus thermal compensation system, the optimally corrected residual optical phase shift can be quite different from a lens. Phase maps form the TCS group finite element simulations have been used in the MSRC case to compute the interferometer behavior. Two different configurations are considered, corresponding to the optimal compensation using only one ring pattern or using two independent ring patterns [4]. The residual optical path lengths are shown in fig. 42.

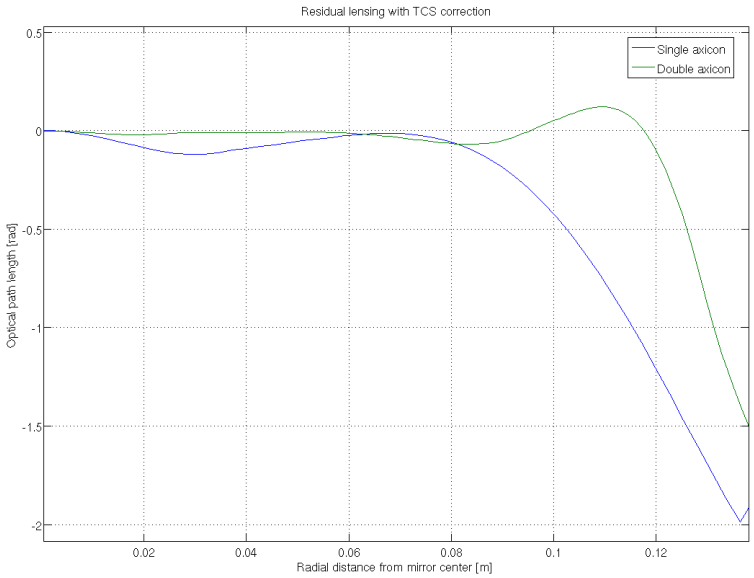


Figure 42: Residual optical path lengths for optimally compensated input mirrors with two different TCS configurations.

The two phase maps have been used to define the input mirror thermal lensing, computing the lens matrix from them. To correctly reproduce the phase map a large number of high order modes were necessary $n + m \leq 20$. It is likely that this large order was not really needed for the simulation but it was in any case used. The same lensing profile has been used for both input mirrors, since differential effects are not very important for MSRC.

The results is shown in fig. 43 where the DARM to dark fringe transfer function is shown. With the double axicon (double ring) configuration all thermal lensing is effectively compensated and no loss in sensitivity is registered. With the single axicon configuration the compensation is not perfect and the loss in sensitivity is comparable to a residual focal length of about 70 km.

The following table lists recycling gains computed in the different configurations:

| | **Carrier total** | **Carrier** $TEM_{00}$ | **Sideband total** | **Sideband** $TEM_{00}$ |
|---|---|---|---|---|
| No thermal effects | 23.54 | 23.54 | 97.99 | 97.99 |
| Single axicon | 23.21 | 23.18 | 31.00 | 23.51 |
| Double axicon | 23.48 | 23.48 | 81.58 | 71.28 |

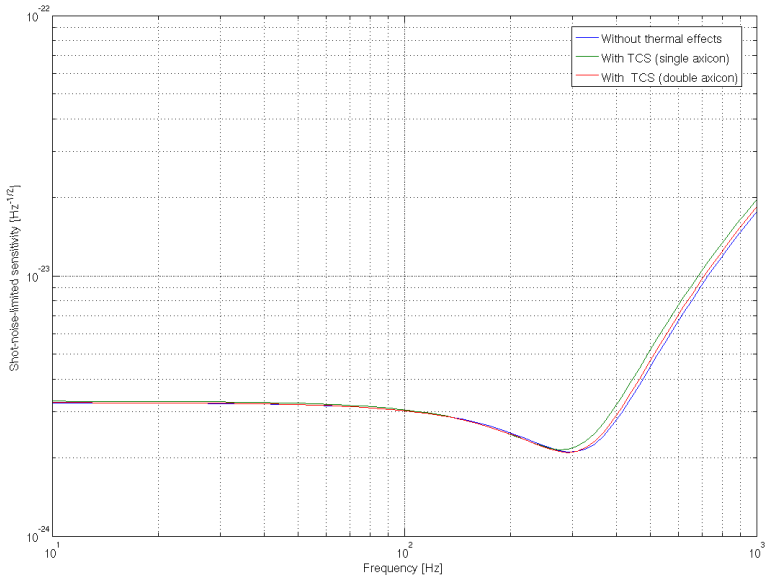


Figure 43: Shot-noise-limited sensitivity with different thermal compensations.

# 10 Conclusions

The first important result of these simulations is that there is no significant difference in sensitivity to thermal lensing between the bi-concave of plane-concave arm configurations, both in the marginally stable of non-degenerate recycling cavities.

The second important point is the need to distinguish between common mode and differential mode thermal lensings.

For what concerns common mode lensings, they affect mainly the power recycling cavity. For what concerns the carrier, MSRC maintains good recycling gain up to about 100 mW (27 km residual lensing), while NDRC can sustain stronger effects. The main difference between the two cases is however well visible in the radio-frequency sideband behavior: NDRC always maintains a good recycling gain even for large common lensings, while MSRC quickly looses power.

The situation is different when considering differential lensings. The carrier is not affected by differential lensing in both configuration. MSRC is also insensitive to differential lensing for what concerns the sidebands. NDRC are instead strongly sensitive to differential lensing, depending in a complex way from the optical design. In the worst case the sensitivity to differential lensings can spoil the sideband recycling gains as much as in the MSRC case. Moreover this sensitivity might turn out to be a very large complication for the lock acquisition.

The two cavities behavior in terms of shot-noise-limited sensitivity is also different. Marginally stable cavities are sensitive only to common mode lensings. However the loss in sensitivity is not dramatic as hinted for example by [5]. With a single axicon thermal compensation system one can recover a reasonably good sensitivity, loosing only 10-20% in shot-noise-limited sensitivity. Non degenerate cavities are almost insensitive to common mode lensing, but the effect of differential lensing is not negligible. Even if not as large as the common mode for MSRC, it can become limiting even with rather large residual focal length.

The NDRC intrinsic astigmatism is almost irrelevant for what concerns sideband recycling gain, but it plays a crucial role in the detector sensitivity. The optical design must be carefully studied, but to avoid spoiling significantly the sensitivity the incidence angle on SRC mirrors must be maintained as small as possible and in any case smaller than 1.5 degrees. With about 1.6-1.7 degrees the loss in sensitivity is comparable to what one gets with MSRC and single axicon TCS.

Finally a very good behavior of MSRC both in terms of sideband recycling gain and sensitivity can be recovered using realistic advanced TCS configurations.

# References

[1] G. Vajente, *Modal Interferometer Simulation*, VIR-0142A-10 (2010) 1

[2] A. E. Siegman, *Lasers*, University Science Book, Mill Valley California (1986) 2

[3] The Virgo Collaboration, *Advanced Virgo Baseline Design*, VIR-027A-09 (2009) 9, 13

[4] V. Fafone, A. Rocchi et al. *TCS status and planning*, VIR-0101A-10 41

[5] Y. Pan, *Optimal degeneracy for the signal-recycling cavity in advanced LIGO*, arXiv:gr-qc/0608128 v1 (2006) 43